Fig. 5. Histological examination of developing kidneys in control (A, C, E, and G) and $Taz^{lacZ/lacZ}$ (B, D, F, and H) embryos. A and B: at *embryonic day 13.5*, branching of ureteric buds and formation of renal vesicles and comma- and S-shaped bodies are observed in $Taz^{lacZ/lacZ}$ (B) as well as wild-type and $Taz^{+/lacZ}$ (A) kidneys. C and D: at *embryonic day 15.5*, dilatation of Bowman's capsules (arrows) and adjacent tubules (arrowheads) are detected in $Taz^{lacZ/lacZ}$ kidneys (D) but not in wild-type kidneys (C). E–H: at *embryonic day 18.5*, the atrophic medulla contains multiple cysts of various sizes in $Taz^{lacZ/lacZ}$ kidneys (F and H). The pelvis is dilated and the papilla is not well formed (F). These changes are not observed in wild-type kidneys (E and G). The nephrogenic zone is present in the outer cortex just beneath the capsule in $Taz^{lacZ/lacZ}$ (H) and wild-type (G) kidneys. Scale bars indicate 100 μm (A–D, G, and H) and 500 μm (E and F).

underlie the renal phenotypes in $Taz^{lacZ/lacZ}$ kidneys. To explore the basis for disturbed water metabolism, we investigated the expression of genes and proteins that are involved in renal water transport. Although the urinary concentration defects in $Taz^{lacZ/lacZ}$ mice were resistant to exogenous vasopressin, real-time RT-PCR analysis showed that the expression of the arginine vasopressin receptor 2 gene (*Avpr2*) was largely unaffected in $Taz^{lacZ/lacZ}$ kidneys (Fig. 9A). The expression of aquaporin (*Aqp-1*, *-2*, and *-3*) water channels that are involved in renal water reabsorption (28) was not different among wild-type, heterozygous, and homozygous mutant kidneys (Fig. 9B). Immunostaining demonstrated that aquaporin-3 was localized in the basolateral membrane of epithelial cells in both $Taz^{lacZ/lacZ}$ and control $Taz^{+/lacZ}$ kidneys (Fig. 9, C and D),

indicating that the polarity of aquaporin-3 localization in $Taz^{lacZ/lacZ}$ epithelial cells was intact. In $Taz^{lacZ/lacZ}$ kidneys, aquaporin-3 was expressed in many noncystic tubules and a few cysts (Fig. 9D), indicating an origin from the renal collecting ducts. Aquaporin-2 was also expressed similarly in collecting ducts in heterozygous and homozygous kidneys at *embryonic day 18.5* (Fig. 9, E and F). These results indicated that the renal phenotype of $Taz^{lacZ/lacZ}$ mice was not caused by changes in the expression of *Avpr2* or aquaporins.

DISCUSSION

In the present study, we demonstrate that a null mutation of *Taz* results in the formation of bilateral multicystic kidneys and
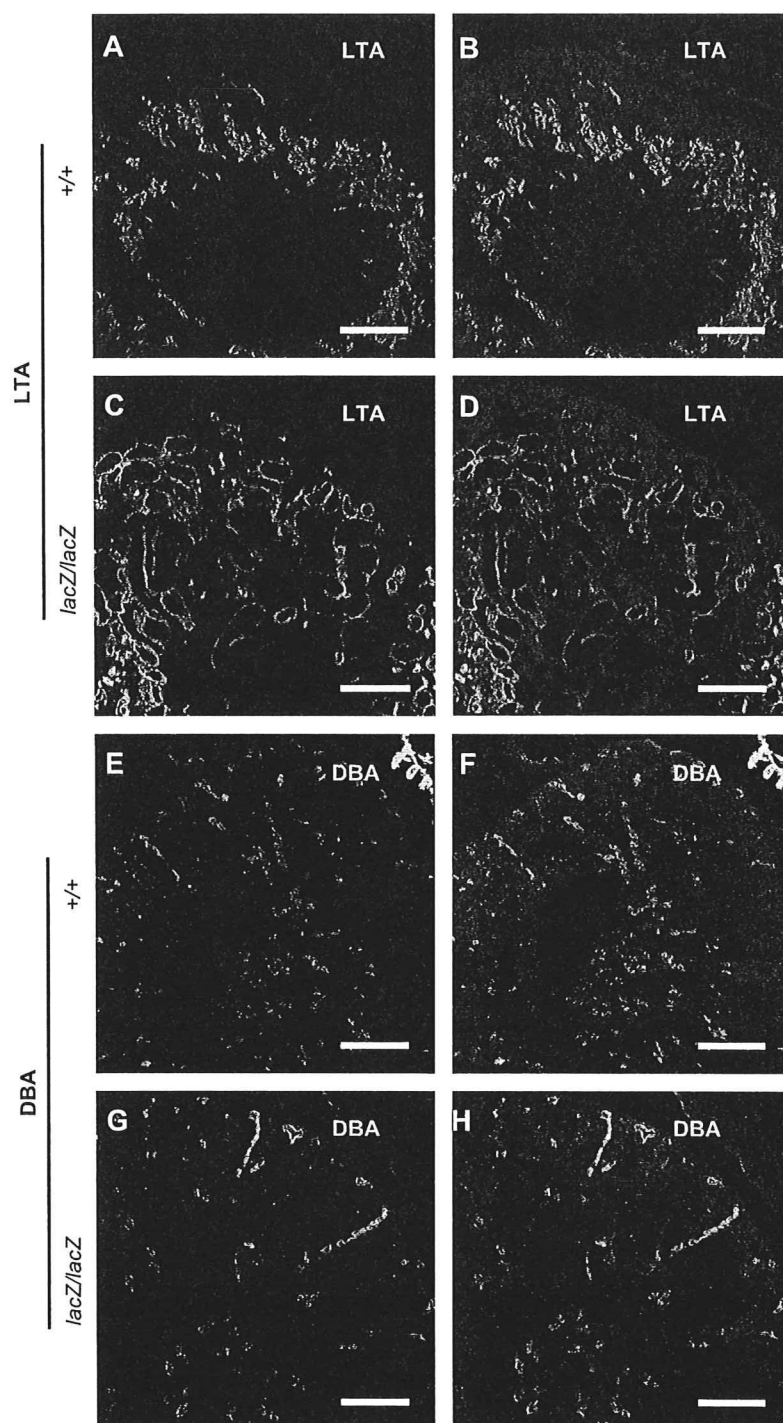
Fig. 6. Proximal tubular dilatation leading to cyst formation in $Taz^{lacZ/lacZ}$ embryos. Sections were stained with *Lotus tetragonolobus* agglutinin (LTA; *A–D*) or *Dolichos biflorus* agglutinin (DBA; *E–H*) in wild-type (*A, B, E,* and *F*) and $Taz^{lacZ/lacZ}$ (*C, D, G,* and *H*) kidneys at *embryonic day 18.5*. *B, D, F,* and *H* show costaining with propidium iodide and lectins. Epithelial cells lining dilated tubules and cysts stain positive with LTA but not with DBA in $Taz^{lacZ/lacZ}$ kidneys. Scale bars indicate 250 μm.

diffuse emphysematous changes in the lung. Renal cysts mainly originate from the glomeruli and proximal tubules around *embryonic day 15.5*, as revealed by histological features and lectin marker staining. Later, the renal changes are accompanied by pelvic dilatation and atrophy of the medulla, indicating hydronephrosis. After birth, only one-fifth of TAZ-deficient homozygotes grow to adulthood. The early mortality may be due to water and electrolyte imbalance and/or respiratory insufficiency. Surviving mutants demonstrate progressive renal changes with massive polyuria. The renal phenotype of
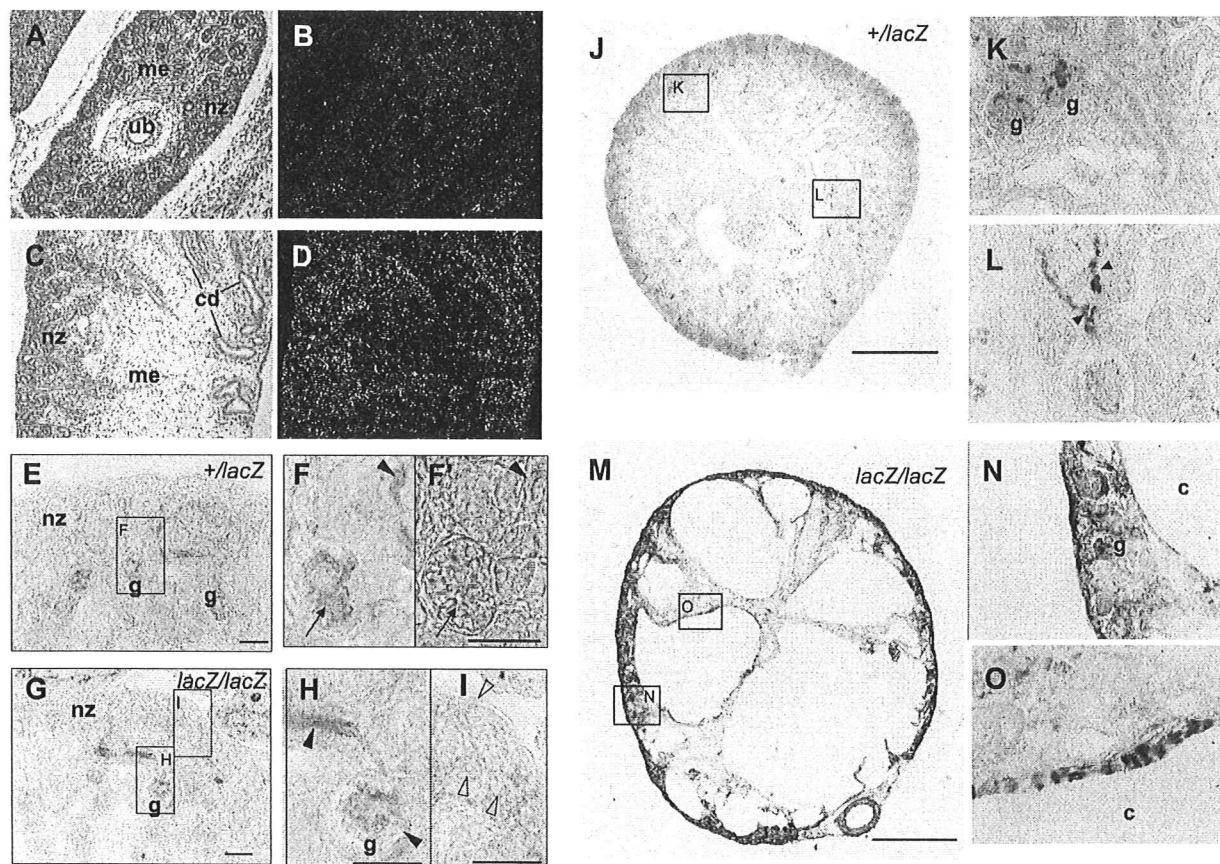
Fig. 7. *Taz* expression during metanephric development. *A–D*: in situ hybridization of mouse embryonic kidneys with probes for *Taz*. Brightfield (*A* and *C*) and darkfield (*B* and *D*) images of *embryonic day 14.5* (*A* and *B*) and *embryonic day 16.5* (*C–F*) kidneys are shown. *A* and *B*: at *embryonic day 14.5*, *Taz* transcripts are diffusely detected in metanephric mesenchymal and epithelial cells and the ureteric bud. *C* and *D*: at *embryonic day 16.5*, *Taz* is expressed in mesenchymal and epithelial cells in the nephrogenic zone. *Taz* is also expressed in the collecting ducts. *E–O*: β-galactosidase activity in $Taz^{+/lacZ}$ (*E*, *F*, and *J–L*) and $Taz^{lacZ/lacZ}$ (*G–I* and *M–O*) kidneys at *embryonic day 16.5* (*E–I*) and *day 0* postpartum (P0; *J–O*). *E*, *F*, and *F'*, in *embryonic day 16.5* $Taz^{+/lacZ}$ kidneys, X-gal staining (blue) is observed in glomeruli (arrows) and CD31-stained (brown) capillary endothelial cells (arrowheads). X-gal staining with (*F*) and without (*F'*) CD31 staining is shown. *G–I*: in *embryonic day 16.5* $Taz^{lacZ/lacZ}$ kidneys, X-gal staining is observed in stromal(-like) cells (open arrowheads in *I*) as well as in glomeruli and capillary endothelial cells (filled arrowheads in *H*). *J–L*: in P0 $Taz^{+/lacZ}$ kidneys, scattered X-gal staining is observed in glomeruli (*K*) and capillary endothelial cells (*L*). *M–O*: in P0 $Taz^{lacZ/lacZ}$ kidneys, X-gal staining is observed in outer cortical stromal cells, glomeruli, and capillaries (*N*). Some cysts are lined by X-gal-positive cells (*O*). Sections of P0 kidney were counterstained with Orange G. c, cyst; cd, collecting duct; g, glomerulus; me, mesenchyme; nz, nephrogenic zone; ub, ureteric bud. Scale bars indicate 50 μm (*E* and *I*) and 500 μm (*J* and *M*).

TAZ-deficient mice is reminiscent of human renal cystic diseases, as represented by PKD, but is distinct in that it manifests as severe hydronephrosis and urinary concentration defects.

Comparison of the renal phenotype of TAZ-deficient mice to human cystic kidney diseases. In human ADPKD, the epithelial-lined cysts originate from any segment of the nephron and collecting ducts, and in ARPKD the cysts mainly originate from the collecting ducts (3, 10). In contrast, the cysts in TAZ-deficient kidneys mainly originate from the glomeruli and proximal tubules. However, patients with early onset ADPKD may develop glomerular cysts, suggesting that cyst formation in the proximal nephrons may be an early manifestation of ADPKD (11. 15). Consistently, *Pkd1*-null mice start to exhibit cyst formation at *embryonic day 15.5* in the proximal tubule (20). Other animal models of PKD, such as the *cpk/cpk* mice and the Han:SPRD *cy/+* rats, have also shown cysts originating predominantly from the proximal tubule (39). Studies of human fetuses with ARPKD have shown cysts originating from proximal tu-

bules. Thus the renal phonotype of TAZ-deficient mice may recapitulate the early phase of human PKD.

However, no apparent differences in the expression of PKD genes, *Pkd1*, *Pkd2*, and *Pkhd1*, are detected in the kidneys of wild-type and TAZ-deficient embryos before birth. This finding indicates that cyst formation in TAZ-deficient kidneys is not due to changes in the expression of these cystic disease genes. Polycystin-1 and -2, proteins encoded by ADPKD genes *PKD1* and *PKD2*, respectively, are membrane glycoproteins that can associate with each other to form a complex in the primary cilium of renal epithelial cells (2, 10, 19). The polycystin complex is implicated in cell cycle regulation, intracellular calcium regulation, and maintenance of cellular polarity (2, 10, 19). Polyductin/fibrocystin, the protein encoded by *PKHD1*, is also a large transmembrane protein. Considering the possible interaction of TAZ with membrane-associated PDZ domain-containing proteins, it may still be possible that TAZ and the cystic disease proteins share a common pathway
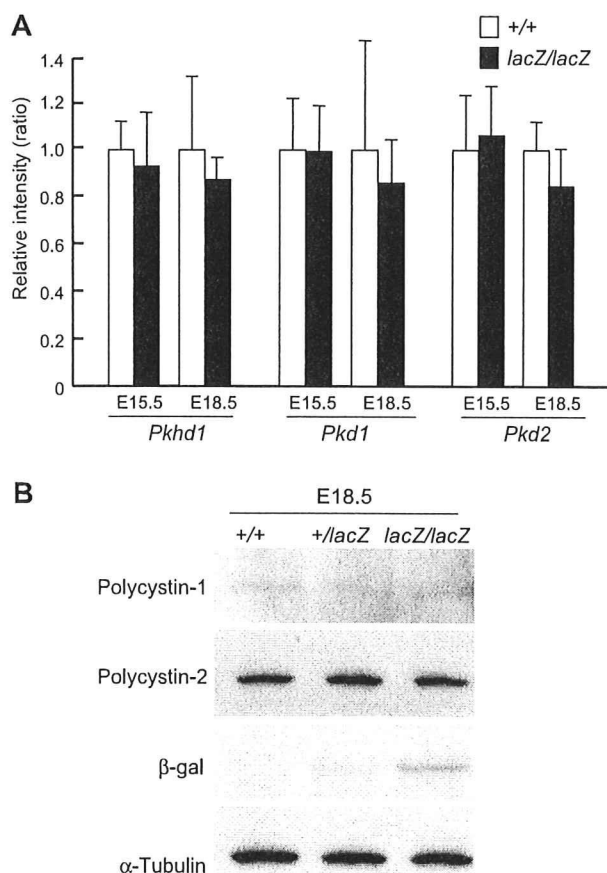
A

B

Fig. 8. Real-time RT-PCR analysis and Western blotting of cystic disease genes and proteins. *A*: real-time RT-PCR. Total RNA samples were prepared from *embryonic day 15.5* and *18.5* wild-type (+/+) and homozygous (*lacZ/lacZ*) kidneys. The abundance of transcripts for *Pkd1*, *Pkd2*, and *Pkhd1* was measured relative to the internal control *Gapdh*. Error bars indicate SDs of the mean ($n = 5$). For all threes genes at both stages, the expression in homozygous mutant kidneys is not statistically different from wild-type kidney ($P > 0.05$). *B*: Western blotting for polycystin-1 and polycystin-2. Protein levels of polycystin-1 and -2 are not different among wild-type, $Taz^{+/lacZ}$, and $Taz^{lacZ/lacZ}$ kidneys at *embryonic day 18.5*. Blotting for β-galactosidase shows intensities corresponding to the copy number of the *lacZ* gene. Blotting for α-tubulin serves as an internal control.

involved in normal epithelial function and structural integrity. However, taken together with the pathological differences from human PKD, distinct mechanisms may be involved in the renal phenotype of TAZ-deficient mice.

Recently, Hossain et al. (16) also reported the development of cystic kidney disease in TAZ/Wwtr1-deficient mice. Their study suggested that the loss of renal cilia integrity and downregulation of several genes, including *Pkhd1*, might be associated with the development of renal cysts in TAZ-deficient mice. Independently, Tian et al. (35) have reported that polycystin-2 is overexpressed in adult TAZ-deficient kidneys as a result of decreased ubiquitin-mediated degradation. In the present study, no changes in fibrocystin or polycystin-2 expression are observed in TAZ-deficient kidneys during the prenatal stage, when cyst formation starts. Abnormalities in fibrocystin

and polycystin-2 may be involved in later stages of disease progression rather than initial cystogenesis.

Comparison of the renal phenotype of TAZ-deficient mice with human nephrogenic diabetes insipidus. A major difference between the renal phenotype of TAZ-deficient mice and human PKD is the presence of severely dilated calyces and massive polyuria. Although humans with ADPKD and ARPKD may have urinary concentration defects (6, 21), severe polyuria and hydronephrosis are not typical clinical features. TAZ-deficient mice have normal daily excretion of sodium and potassium, indicating that tubular electrolyte reabsorption is well preserved. The relatively low urine osmolality compared with wild-type together with impaired response to exogenous vasopressin are characteristic of nephrogenic diabetes insipidus. Hydronephrosis may be secondary to polyuria, as seen in congenital progressive hydronephrosis (*cph*) mutant mice (22). Thus the renal phenotype of TAZ-deficient mice is characterized by two distinct pathophysiological processes, cyst formation and urinary concentration defects.

Nephrogenic diabetes insipidus is caused by the inability of the renal collecting ducts to reabsorb water in response to vasopressin. About 90% of affected patients have mutations in the *AVPR2* gene, whereas the remaining 10% of patients are caused by *AQP2* gene mutations (28). However, TAZ-knockout kidneys do not show major abnormalities in the levels of expression of *Avpr2*, *Aqp2*, and *Aqp3*. In addition, the apical-basolateral polarity of aquaporin-2 and aquaporin-3 is preserved in both cystic and noncystic collecting ducts at embryonic and postnatal stages. These findings suggest that the polyuria and hydronephrosis in TAZ-deficient mice do not arise from major defects in the expression or localization of the V_2 vasopressin receptor, aquaporin-2, or aquaporin-3. Elucidation of the mechanism underlying the concentration defects in TAZ-deficient kidney may reveal novel pathways regulating renal water transport.

Possible requirement of TAZ for normal kidney development. The kidney develops through reciprocal interactions between the metanephric mesenchyme and the ureteric bud epithelium during embryogenesis (8, 36, 40). The ureteric bud grows into the metanephric mesenchyme and branches to form the collecting duct system while the mesenchyme adjacent to the tips of the ureteric bud is induced to condense and undergo a mesenchymal-to-epithelial transition. The resultant renal vesicle further differentiates into comma- and then S-shaped bodies. Morphogenesis and patterning of the epithelial structures lead to the formation and functional maturation of nephron segments including the glomerulus, the proximal tubule, the loop of Henle, and the distal tubule. Recent advances in gene targeting experiments have greatly contributed to the understanding of molecular mechanisms underlying the early "inductive" phase of kidney development. However, it remains largely unknown how each nephron segment is specified and functionally matures during the late phase of kidney development.

In situ hybridization and β-galactosidase staining demonstrated that *Taz* is diffusely expressed throughout the kidney. *Taz* expression is most intense in the nephrogenic zone during kidney development and is found in both mesenchymal and epithelial cells. *Taz* is not restricted to a specific segment of the nephron. Capillary endothelial cells also express *Taz*. *LacZ* expression is relatively scant and scattered compared with the pattern of in situ hybridization. This difference may be caused

Fig. 9. Expression of genes involved in water transport. A: real-time RT-PCR. Total RNA samples were prepared from *embryonic day 18.5* and 2-wk-old wild-type (+/+) and homozygous (*lacZ/lacZ*) kidneys. The abundance of transcripts for Avpr2 was measured relative to the internal control Gapdh. Error bars indicate SDs of the mean; $n = 5$ (+/+) and 5 (*lacZ/lacZ*) at *embryonic day 18.5*; $n = 4$ (+/+) and 3 (*lacZ/lacZ*) at 2 wk; $n = 8$ (+/+) and 6 (*lacZ/lacZ*) at 8–12 wk; $n = 4$ (+/+) and 4 (*lacZ/lacZ*) at 20–26 wk. No statistically significant difference is detected in the expression of Avpr2 between +/+ and *lacZ/lacZ* kidneys ($P > 0.05$). B: RT-PCR analysis of *Aquaporin-1*, -2, and -3 expression. Total RNA samples were prepared from *embryonic day 18.5* wild-type (+/+), heterozygous (+/*lacZ*), and homozygous (*lacZ/lacZ*) kidneys. The levels of *Aquaporin-1*, -2, and -3 transcripts are not different among wild-type, heterozygous, and homozygous kidneys. RT-PCR for Gapdh served as an internal control. C–F: immunofluorescence staining of aquaporins. Sections were stained for aquaporin-3 (C and D) or aquaporin-2 (E and F) in Taz$^{+/lacZ}$ (C and E) and Taz$^{lacZ/lacZ}$ (D and F) kidneys at *embryonic day 18.5*. All sections were costained with 4',6-diamidine-2-phenylindole. Aquaporin-3 is localized in the basolateral membrane of epithelial cells in some cysts (arrow) as well as in noncystic tubules (arrowheads) in Taz$^{lacZ/lacZ}$ kidneys. Aquaporin-2 is also expressed similarly in collecting ducts in heterozygous and homozygous kidneys. Scale bars indicate 10 μm.
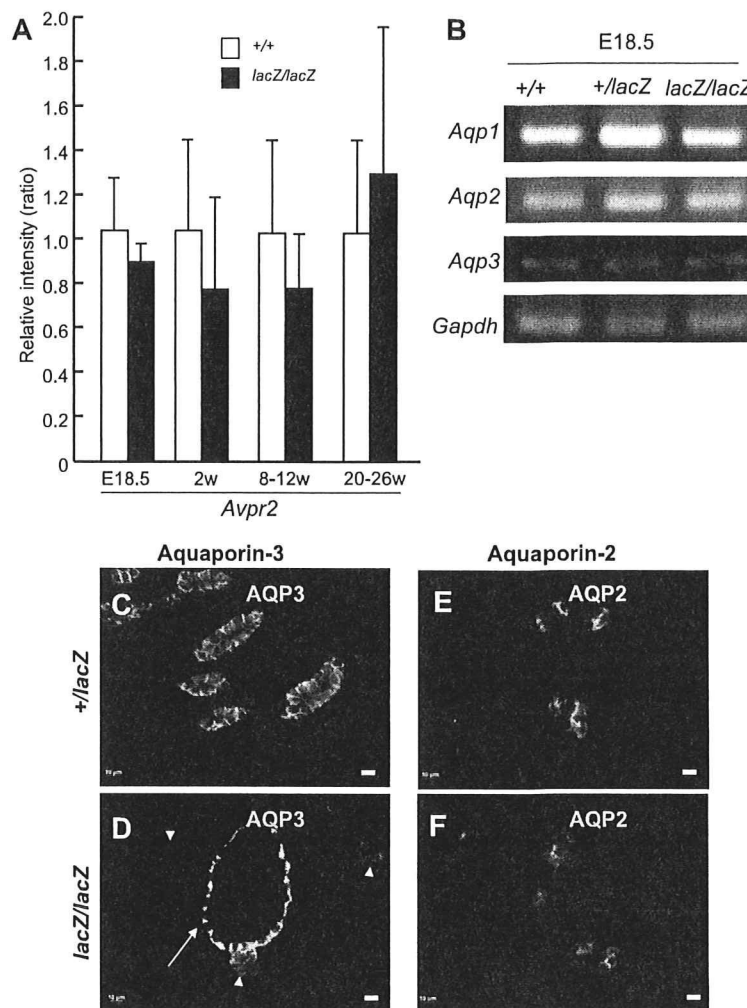
by deletion or disruption of critical enhancer element(s) during the generation of the targeted mutation.

In TAZ-deficient kidneys, most, but not all, of the cyst epithelium is *lacZ*-negative. In contrast, stromal cells, especially in the nephrogenic zone, show strong *lacZ* expression in TAZ-deficient kidneys. This finding indicates that TAZ may be crucial for gene expression in stromal cells supporting normal nephric development.

Pulmonary emphysematous changes in TAZ-deficient mice. In addition to renal cyst formation, TAZ-deficient mice demonstrate severely enlarged air spaces in the lung. This finding is morphologically reminiscent of human pulmonary emphysema, whose genetic pathogenesis is poorly understood. Only a congenital form of emphysema is known to be caused by a deficiency of α-antitrypsin, but its expression was not affected in TAZ-deficient mice (our unpublished data).

Pulmonary emphysema, as a manifestation of COPD, is regarded as a multifactorial disorder triggered by environmental factors such as cigarette smoking and pollutants. Although genetic factors involved in protease/antiprotease balance have been considered as possible determinants of susceptibility to emphysematous changes, the molecular pathogenesis is still unknown. In mice, emphysema-like pulmonary changes can be caused by deficiency in surfactant proteins SP-C or SP-D, possibly through increased activity of matrix metalloproteases (9, 38). Interestingly, TAZ has been reported to be a coactivator for the transcription factor TTF-1/Nkx2.1 and upregulates the expression of SP-C in respiratory epithelial cells (5). However, SP-C expression was not apparently affected in TAZ-deficient lungs (unpublished observations), so different mechanisms may generate the emphysematous changes in TAZ-deficient lungs.

The coexistence of renal and pulmonary abnormalities observed in TAZ-deficient mice has not been described before. However, there are similarities in the embryonic development of the kidney and lung. Both involve common processes, e.g., branching morphogenesis and common signaling pathways such as sonic hedgehog, fibroblast growth factor, and bone morphogenetic protein (17, 41). These similarities raise the possibility that TAZ may be an effector in a common pathway that is involved in both lung and kidney development. Although the apical-basolateral polarity of epithelial cells in collecting ducts is not impaired in TAZ-deficient kidneys, further examination of the processes of epithelial tubule formation in TAZ-deficient kidneys and lungs may reveal a

common mechanism for organogenesis and pathogenesis of human diseases.

REFERENCES

1. **Barnes PJ.** New concepts in chronic obstructive pulmonary disease. *Annu Rev Med* 54: 113–129, 2003.
2. **Benezra R.** Polycystins: inhibiting the inhibitors. *Nat Cell Biol* 7: 1064–1065, 2005.
3. **Bisceglia M, Galliani CA, Senger C, Stallone C, Sessa A.** Renal cystic diseases: a review. *Adv Anat Pathol* 13: 26–56, 2006.
4. **Chen Q, Takahashi S, Zhong S, Hosoda C, Zheng HY, Ogushi T, Fujimura T, Ohta N, Tanoue A, Tsujimoto G, Kitamura T.** Function of the lower urinary tract in mice lacking alpha1d-adrenoceptor. *J Urol* 174: 370–374, 2005.
5. **Cui CB, Cooper LF, Yang X, Karsenty G, Aukhil I.** Transcriptional coactivation of bone-specific transcription factor Cbfa1 by TAZ. *Mol Cell Biol* 23: 1004–1013, 2003.
6. **D'Angelo A, Mioni G, Ossi E, Lupo A, Valvo E, Maschio G.** Alterations in renal tubular sodium and water transport in polycystic kidney disease. *Clin Nephrol* 3: 99–105, 1975.
7. **Deen PMT.** Mouse models for congenital nephrogenic diabetes insipidus: what can we learn from them? *Nephrol Dial Transplant* 22: 1023–1026, 2007.
8. **Dressler GR.** Tubulogenesis in the developing mammalian kidney. *Trends Cell Biol* 12: 390–395, 2002.
9. **Glasser SW, Detmer EA, Ikegami M, Na CL, Stahlman MT, Whitsett JA.** Pneumonitis and emphysema in sp-C gene targeted mice. *J Biol Chem* 278: 14291–14298, 2003.
10. **Guay-Woodford LM.** Murine models of polycystic kidney disease: molecular and therapeutic insights. *Am J Physiol Renal Physiol* 285: F1034–F1049, 2003.
11. **Gusmano R, Caridi G, Marini M, Perfumo F, Ghiggeri GM, Piaggio G, Ceccherini I, Seri M.** Glomerulocystic kidney disease in a family. *Nephrol Dial Transplant* 17: 813–818, 2002.
12. **Hogg JC.** Pathophysiology of airflow limitation in chronic obstructive pulmonary disease. *Lancet* 364: 709–721, 2004.
13. **Hong JH, Hwang ES, McManus MT, Amsterdam A, Tian Y, Kalmukova R, Mueller E, Benjamin T, Spiegelman BM, Sharp PA, Hopkins N, Yaffe MB.** TAZ, a transcriptional modulator of mesenchymal stem cell differentiation. *Science* 309: 1074–1078, 2005.
14. **Hong JH, Yaffe MB.** TAZ: a β-catenin-like molecule that regulates mesenchymal stem cell differentiation. *Cell Cycle* 5: 176–179, 2006.
15. **Horie S.** ADPKD: molecular characterization and quest for treatment. *Clin Exp Nephrol* 9: 282–291, 2005.
16. **Hossain Z, Ali SM, Ko HL, Xu J, Ng CP, Guo K, Qi Z, Ponniah S, Hong W, Hunziker W.** Glomerulocystic kidney disease in mice with a targeted inactivation of Wwtr1. *Proc Natl Acad Sci USA* 104:1631–1636, 2007.
17. **Hu MC, Rosenblum ND.** Genetic regulation of branching morphogenesis: lessons learned from loss-of-function phenotypes. *Pediatr Res* 54: 433–438, 2003.
18. **Kanai F, Marignani PA, Sarbassova D, Yagi R, Hall RA, Donowitz M, Hisaminato A, Fujiwara T, Ito Y, Cantley LC, Yaffe MB.** TAZ: a novel transcriptional co-activator regulated by interactions with 14-3-3 and PDZ domain proteins. *EMBO J* 19: 6778–6791, 2000.
19. **Li X, Luo Y, Starremans PG, McNamara CA, Pei Y, Zhou J.** Polycystin-1 and polycystin-2 regulate the cell cycle through the helix-loop-helix inhibitor Id2. *Nat Cell Biol* 7: 1102–1112, 2005.
20. **Lu W, Peissel B, Babakhanlou H, Pavlova A, Geng L, Fan X, Larson C, Brent G, Zhou J.** Perinatal lethality with kidney and pancreas defects in mice with a targetted Pkd1 mutation. *Nat Genet* 17: 179–181, 1997.
21. **Martinez-Maldonado M, Yium JJ, Eknoyan G, Suki WN.** Adult polycystic kidney disease: studies of the defect in urine concentration. *Kidney Int* 2: 107–113, 1972.
22. **McDill BW, Li SZ, Kovach PA, Ding L, Chen F.** Congenital progressive hydronephrosis (cph) is caused by an S256L mutation in aquaporin-2 that affects its phosphorylation and apical membrane accumulation. *Proc Natl Acad Sci USA* 103: 6952–6957, 2006.
23. **Mochizuki T, Wu G, Hayashi T, Xenophontos SL, Veldhuisen B, Saris JJ, Reynolds DM, Cai Y, Gabow PA, Pierides A, Kimberling WJ, Breuning MH, Deltas CC, Peters DJ, Somlo S.** PKD2, a gene for polycystic kidney disease that encodes an integral membrane protein. *Science* 272: 1339–1342, 1996.
24. **Murakami M, Nakagawa M, Olson EN, Nakagawa O.** A WW domain protein TAZ is a critical coactivator for TBX5, a transcription factor implicated in Holt-Oram syndrome. *Proc Natl Acad Sci USA* 102: 18034–18039, 2005.
25. **Murakami M, Tominaga J, Makita R, Uchijima Y, Kurihara Y, Nakagawa O, Asano T, Kurihara H.** Transcriptional activity of Pax3 is co-activated by TAZ. *Biochem Biophys Res Commun* 339: 533–539, 2006.
26. **Nagy A, Gertsenstein M, Vintersten K, Behringer R.** *Manipulating the Mouse Embryo: A Laboratory Manual* (3rd ed.). Cold Spring Harbor, NY: Cold Spring Harbor Laboratory, 2003.
27. **Nakagawa O, Nakagawa M, Richardson JA, Olson EN, Srivastava D.** HRT1, HRT2, and HRT3: a new subclass of bHLH transcription factors marking specific cardiac, somitic, and pharyngeal arch segments. *Dev Biol* 216: 72–84, 1999.
28. **Nielsen S, Frøkiar J, Marples D, Kwon TH, Agre P, Knepper MA.** Aquaporins in the kidney: from molecules to medicine. *Physiol Rev* 82: 205–244, 2002.
29. **Onuchic LF, Furu L, Nagasawa Y, Hou X, Eggermann T, Ren Z, Bergmann C, Senderek J, Esquivel E, Zeltner R, Rudnik-Schoneborn S, Mrug M, Sweeney W, Avner ED, Zerres K, Guay-Woodford LM, Somlo S, Germino GG.** PKHD1, the polycystic kidney and hepatic disease 1 gene, encodes a novel large protein containing multiple immunoglobulin-like plexin-transcription-factor domains and parallel beta-helix 1 repeats. *Am J Hum Genet* 70: 1305–1317, 2002.
30. **Park KS, Whitsett JA, Di Palma T, Hong JH, Yaffe MB, Zannini M.** TAZ interacts with TTF-1 and regulates expression of surfactant protein-C. *J Biol Chem* 279: 17384–17390, 2004.
31. **Shao X, Johnson JE, Richardson JA, Hiesberger T, Igarashi P.** A minimal Ksp-cadherin promoter linked to a green fluorescent protein reporter gene exhibits tissue-specific expression in the developing kidney and genitourinary tract. *J Am Soc Nephrol* 13: 1824–1836, 2002.
32. **The European Polycystic Kidney Disease Consortium.** The polycystic kidney disease 1 gene encodes a 14 kb transcript and lies within a duplicated region on chromosome 16. *Cell* 77: 881–894, 1994.
33. **The International Polycystic Kidney Disease Consortium.** Polycystic kidney disease: the complete structure of the PKD1 gene and its protein. *Cell* 81: 289–298, 1995.
34. **Thurlbeck WM.** Measurement of pulmonary emphysema. *Am Rev Respir Dis* 95: 752–764, 1967.
35. **Tian Y, Kolb R, Hong JH, Carroll J, Li D, You J, Bronson R, Yaffe MB, Zhou J, Benjamin T.** TAZ promotes PC2 degradation through a SCFβ-Trcp E3 ligase complex. *Mol Cell Biol* 27: 6383–6395, 2007.
36. **Vainio S, Lin Y.** Coordinating early kidney development: lessons from gene targeting. *Nat Rev Genet* 3: 533–543, 2002.
37. **Ward CJ, Hogan MC, Rossetti S, Walker D, Sneddon T, Wang X, Kubly V, Cunningham JM, Bacallao R, Ishibashi M, Milliner DS, Torres VE, Harris PC.** The gene mutated in autosomal recessive polycystic kidney disease encodes a large, receptor-like protein. *Nat Genet* 30: 259–269, 2002.
38. **Wert SE, Yoshida M, LeVine AM, Ikegami M, Jones T, Ross GF, Fisher JH, Korfhagen TR, Whitsett JA.** Increased metalloproteinase activity, oxidant production, and emphysema insurfactant protein D gene-inactivated mice. *Proc Natl Acad Sci USA* 97: 5972–5977, 2000.
39. **Witzgall R.** The proximal tubule phenotype and its disruption in acute renal failure and polycystic kidney disease. *Exp Nephrol* 7: 15–19, 1999.
40. **Yu J, McMahon AP, Valerius MT.** Recent genetic studies of mouse kidney development. *Curr Opin Genet Dev* 14: 550–557, 2004.
41. **Zegers MM, O'Brien LE, Yu W, Datta A, Mostov KE.** Epithelial polarity and tubulogenesis in vitro. *Trends Cell Biol* 13: 169–176, 2003.

ELSEVIER

Maintenance of genomic methylation patterns during preimplantation development requires the somatic form of DNA methyltransferase 1

Yukiko Kurihara [a,*], Yumiko Kawamura [a], Yasunobu Uchijima [a], Tomokazu Amamo [b],
Hiroshi Kobayashi [a], Tomoichiro Asano [a,c], Hiroki Kurihara [a]

[a] Department of Physiological Chemistry and Metabolism, Graduate School of Medicine, The University of Tokyo, 7-3-1 Hongo, Bunkyo-ku, Tokyo 113-0033, Japan
[b] Department of Developmental Medical Technology (Sankyo), Graduate School of Medicine, The University of Tokyo, Tokyo 113-0033, Japan
[c] Department of Biomedical Chemistry, Hiroshima University Graduate School of Biomedical Sciences, Hiroshima 734-8551, Japan

Abstract

DNA methylation at cytosine residues in CpG dinucleotides is a component of epigenetic marks crucial to mammalian development. In preimplantation stage embryos, a large part of genomic DNA is extensively demethylated, whereas the methylation patterns are faithfully maintained in certain regions. To date, no enzymes responsible for the maintenance of DNA methylation during preimplantation development have been identified except for the oocyte form of DNA (cytosine-5)-methyltransferase 1 (Dnmt1o) at the 8-cell stage. Herein, we demonstrate that the somatic form of Dnmt1 (Dnmt1s) is present in association with chromatin in MII-stage oocytes as well as in the nucleus throughout preimplantation development. At the early one-cell stage, Dnmt1s is asymmetrically localized in the maternal pronuclei. Thereafter, Dnmt1s is recruited to the paternal genome during pronuclear maturation. During the first two cell cycles after fertilization, Dnmt1s is exported from the nucleus in the G2 phase in a CRM1/exportin-dependent manner. Antibody microinjection and small interfering RNA-mediated knock-down decreases methylated CpG dinucleotides in repetitive intracisternal A-type particle (IAP) sequences and the imprinted gene *H19*. These results indicate that Dnmt1s is responsible for the maintenance methylation of particular genomic regions whose methylation patterns must be faithfully maintained during preimplantation development.
© 2007 Elsevier Inc. All rights reserved.

Keywords: DNA methylation; DNA methyltransferase; Preimplantation development; Genomic imprinting; Nucleocytoplasmic shuttling

Introduction

DNA methylation at cytosine residues in CpG dinucleotides is a component of epigenetic marks crucial to mammalian development (Jaenisch and Bird, 2003; Li, 2002; Reik et al., 2001). After fertilization, the zygote undergoes extensive demethylation of genomic DNA (Dean et al., 2003; Morgan et al., 2005; Santos and Dean, 2004). Genomic DNA of paternal origin is actively demethylated within several hours after fertilization, whereas the oocyte-derived maternal genome is thought to be passively demethylated, resulting in a parental asymmetry in epigenetic marks (Mayer et al., 2000; Oswald et al., 2000;

Rougier et al., 1998). *De novo* and maintenance DNA methylation throughout the genome is restored around the time of implantation to establish tissue-specific epigenetic states. As for germline development, highly methylated primordial germ cells migrate to the genital ridge and then undergo loss and reacquisition of methylation. Thus, two rounds of demethylation/remethylation events constitute an epigenetic cycle in mammals.

Contrary to the genome-wide loss of DNA methylation, methylation states of certain sequences are well preserved during preimplantation development. For example, the mono-allelic methylation of imprinted genes such as *H19* and *Snrpn* must be faithfully maintained for normal development (Doherty et al., 2002; Tremblay et al., 1997; Warnecke et al., 1998). The intracisternal A-type particle (IAP), a repetitive sequence of retrotransposon, is also resistant to demethylation in preim-

* Corresponding author. Fax: +81 3 5684 4958.
 E-mail address: yuki-tky@umin.net (Y. Kurihara).

plantation embryos (Gaudet et al., 2004; Lane et al., 2003). The methylation of these genes is important for preventing their deregulated activation, which may lead to deleterious consequences such as growth abnormalities and tumorigenesis (Egger et al., 2004; Yoder et al., 1997). However, the mechanism distinguishing methyl-CpG-containing sequences to be demethylated versus those to be maintained in preimplantation embryos remains unknown.

Three enzymes with DNA (cytosine-5)-methyltransferase (Dnmt) activity have been identified in mammals (Bestor, 2000). Dnmt1, a large protein with a molecular mass of 190 kDa, predominantly catalyzes maintenance methylation via binding to proliferating cell nuclear antigen (PCNA) in replication foci during the S phase (Bestor et al., 1988; Chuang et al., 1997; Leonhardt et al., 1992). Two other enzymes, Dnmt3a and Dnmt3b, are mainly responsible for *de novo* methylation that establishes a new DNA methylation state (Okano et al., 1999, 1998). Inactivation of both Dnmt3a and Dnmt3b results in defective *de novo* methylation in embryonic stem cells and early embryos but has no discernable effect on the maintenance of preexisting methylation patterns in postimplantation embryos, indicating that virtually all DNA methylation is maintained by Dnmt1 during postimplantation development (Li et al., 1992; Okano et al., 1999).

Unfertilized oocytes and preimplantation embryos are characterized by the presence of Dnmt1o, an isoform of Dnmt1 (Mertineit et al., 1998). Dnmt1o is distinct from the conventional Dnmt1 expressed in most somatic cells (Dnmt1s) in that it uses the oocyte-specific 5' exon, resulting in the formation of an N-terminally truncated protein with a molecular mass of 175 kDa (Mertineit et al., 1998). During preimplantation development, Dnmt1o protein is translated from oocyte-derived mRNA and is actively retained in the cytoplasm except at the eight-cell stage, when Dnmt1o is transiently translocated to the nucleus (Cardoso and Leonhardt, 1999; Doherty et al., 2002; Howell et al., 2001; Mertineit et al., 1998; Ratnam et al., 2002) Mice homozygous for the Dnmt1o-specific knockout allele were normal, but most heterozygotes from homozygous females were embryonic lethal with a partial loss of methylation at imprinted loci (Howell et al., 2001). In contrast, no Dnmt1s protein has been detected in oocytes and preimplantation embryos, although its transcripts are present (Cardoso and Leonhardt, 1999; Ratnam et al., 2002). These findings have led to the conclusion that Dnmt1o is the only known form of maintenance methyltransferase present in preimplantation embryos and that, except at the eight-cell stage, methylation patterns must be maintained by as yet unknown enzymes (Howell et al., 2001; Ratnam et al., 2002).

Here we demonstrate that Dnmt1s protein is present during preimplantation development. Characteristically, the nuclear localization in 1- and 2-cell stage embryos appears to be controlled by a CRM1/exportin-mediated nucleocytoplasmic shuttling. Furthermore, inactivation of Dnmt1s in preimplantation embryos revealed that it functions as a maintenance DNA methyltransferase for certain genomic regions including imprinted and repetitive genes.

Materials and methods

Collection of oocytes and embryos

Female ICR mice (8–10 weeks old) were superovulated with intraperitoneal injections of 5 IU of pregnant mare serum gonadotropin (PMSG; Teikoku Hormone Mfg.) and, 48 h later, 5 IU of human chorionic gonadotropin (hCG; Teikoku Hormone Mfg.). Oocytes were recovered from the oviducts 20 h after hCG injection, and cumulus cells were extensively dispersed with 1 mg/ml hyaluronidase (Sigma). Preimplantation embryos were obtained from superovulated females mated to ICR males on appropriate days for each cleavage stage. To obtain one-cell embryos at early pronuclear stages, ICSI or *in vitro* fertilization (IVF) was performed on unfertilized oocytes collected as above and sperm obtained from ICR males according to standard procedures. Embryos were cultured in KSOM medium at 37 °C in humidified air containing 5% CO_2.

Plasmids

The mouse Dnmt1s cDNA was cloned by RT-PCR on total RNA from the mouse liver. For glutathione *S*-transferase (GST) fusion protein, a cDNA fragment encoding the N-terminal 118 amino acids of Dnmt1s was subcloned in-frame into the pGEX vector (Amersham Pharmacia Biotech). For a series of enhanced green fluorescence protein (EGFP)-fusion constructs, cDNA fragments encompassing the open reading frame of Dnmt1s and its derivatives were subcloned in-frame into the pEGFP-C2 expression vector (Clontech). Fragments encoding EGFP-Dnmt1 constructs were then subcloned into pBluescript (Stratagene) or pCRII-TOPO (Invitrogen) for *in vitro* transcription. All the constructs were verified by sequencing.

Antibodies

To generate polyclonal antibody against the N-terminal region of Dnmt1s, we prepared fusion proteins between GST and the N-terminal 118 amino acids of Dnmt1s in *Escherichia coli*, and purified them using glutathione-coupled Sepharose beads. The purified GST fusion proteins were injected into rabbits. The antibody, named N48, was affinity-purified using this antigen bound to Affi-Gel 10 (Bio-Rad).

Cell culture and transfection

NIH3T3 cells were cultured in Dulbecco's modified Eagle's medium containing 10% fetal calf serum and antibiotics at 37 °C in 5% CO_2. For transfection of small interfering RNA (siRNA), cells were grown to 50–90% confluence and were treated with mixture of siRNA and OligofectAMINE reagents (Invitrogen) according to the manufacturer's protocol.

Western blotting

A pool of ~500 unfertilized oocytes were lysed in PBS containing 1% Nonidet P-40 and protease inhibitors, and then subjected to 7.5% SDS-PAGE with lysates of NIH3T3 cells. The separated proteins were transferred to a nylon membrane, which was then pre-treated with 3% bovine serum albumin for blocking and incubated with the N48 antibody and treated with anti-rabbit IgG antibody conjugated to horseradish peroxidase (ICN). The protein bands were visualized using an ECL Plus Western Blotting Detection System (Amersham Pharmacia Biotech). Then, the membrane was washed and re-blotted with the H-300 antibody recognizing the C-terminus of Dnmt1 (rabbit, Santa Cruz). The relative amounts of proteins were estimated by densitometry using the ImageJ software (NIH).

Immunostaining

Unfertilized oocytes and preimplantation embryos were freed of the zona pellucida by using acidified Tyrode's medium, fixed for 15 min in 4%

paraformaldehyde in PBS, and permeabilized with 0.2% Triton X-100 in PBS for 5 min at room temperature. After blocking for 30 min in 5% normal donkey serum, the samples were incubated in the same solution with the N48 or H-300 antibodies overnight at 4°C. Then, the samples were washed and stained with the secondary antibodies (FITC- or rhodamine-conjugated donkey anti-rabbit IgG (Jackson Immunoresearch). Staining with rabbit polyclonal anti-GFP antibody (MBL) served as negative control. DNA was visualized by staining with DAPI (1μg/ml) or propidium iodide (50μg/ml). Confocal images were obtained using a Nikon D-ECLIPSE C1 system.

For semi-quantitative analysis of immunofluorescent signals, the pixel value/unit was measured for the nuclear and cytoplasmic signals using ImageJ software (NIH) and the relative nuclear intensity was evaluated by dividing the pixel value/unit of the nuclear signal by that of the cytoplasmic signal. Data were analyzed using analysis of variance (ANOVA) and significance was defined as $P < 0.05$ (Sheffe's F-test).

RNA preparation and microinjection

Preparation and injection of in vitro transcribed mRNA were performed as previously described (Aida et al., 2001). Briefly, plasmids containing EGFP-Dnmt1 fusion constructs were linearized and used as templates for in vitro transcription employing the T7 MessageMachine kit (Ambion). Synthesized RNA was further polyadenylated by yeast poly(A) polymerase (Amersham Biosciences) and resolved in 150 mM KCl with a final concentration of ~100 ng/μl. The diluted RNA was filtered, heated at 90 °C for 1 min and cooled on ice. Then, ~10 pl of the RNA solution were injected into fertilized eggs or two-cell embryos through a glass micropipette. Fluorescent images were obtained and the relative nuclear intensity was evaluated as in the case of immunostaining.

ICSI with microinjection of antibodies

ICSI was performed as previously described (Kimura and Yanagimachi, 1995). Antibodies were premixed in the sperm suspension to be introduced into oocytes. Anti-GST antibody served as a negative control.

RNA interference

Chemically synthesized 27-nt siRNA duplexes with no overhang were commercially obtained (Japan Bio-Service). Two different sequences for Dnmt1s were selected for the generation of siRNA; the sequences for si290 and si322 corresponded to nucleotides 290–316 and 322–348 of mouse Dnmt1s (GenBank accession number NM_010066), respectively. Inv322, a siRNA possessing the inverted sequence of si322, served as a control. Approximately 10 pl of 20 μM siRNA were injected into the cytoplasm of unfertilized eggs, which were subsequently subjected to in vitro fertilization.

DNA methylation analysis

About 20–40 embryos were embedded in one agarose droplet, which was then treated with sodium bisulfite for cytosine modification as described (Olek et al., 1996). Each sample was subdivided into 2–3 tubes and was subjected to two-round nested PCR analysis. PCR primers were synthesized to analyze the methylation status of the *H19* upstream DMD (GenBank accession number U19619, nucleotides 1304–1726) (Tremblay et al., 1997) and the LTR of IAP (GenBank accession number M17551, nucleotides 48–305) (Lane et al., 2003). Amplified PCR products were subcloned into PCRII-TOPO vector and were sequenced. Bisulfite reaction was considered complete when more than 99% of the cytosines were converted to thymines. For IAP, 3–5 clones were sequenced from each PCR template. For *H19*, paternal alleles were distinguished by a single polymorphism in the analyzed region (Tremblay et al., 1997) and one representative sequence (the youngest number of several sequenced clones) was adopted from each template. Primer sequences are available on request.

Statistical analysis was performed by Mann–Whitney's *U*-test for two-group comparison of antibody-injected embryos, and by one-way ANOVA, Sheffe's post hoc analysis for three-group comparison of siRNA-injected embryos. *P* values less than 0.05 were considered significant.

Results

Dnmt1s protein is present in mouse unfertilized oocytes and preimplantation embryos

To test the current assumption that Dnmt1s mRNA is not translated into proteins during preimplantation development, we first raised a rabbit polyclonal antibody against the N-terminal region specific for the Dnmt1s isoform (Fig. 1A). This antibody, named N48, was capable of detecting a single band with a molecular mass of ~190 kDa in Western blot of MII-stage unfertilized oocyte extracts as well as NIH3T3 cell extracts (Fig. 1B). For comparison, the membrane was re-probed with H-300, an antibody recognizing the C-terminal region of both Dnmt1s and Dnmt1o. Signal intensity was adjusted by changing blotting condition and exposure times to allow comparison of the amounts of Dnmt1s and Dnmt1o as below. As expected, H-300 detected ~175-kDa Dnmt1o in unfertilized oocytes and ~190 kDa-Dnmt1s in NIH3T3 cells (Fig. 1B). Using the signal intensities from different volumes (1× and 4×) of NIH3T3 extracts as references, Dnmt1s was estimated to be ~2000-fold less abundant than Dnmt1o in MII-stage unfertilized oocytes. The presence of Dnmt1s was also confirmed with another Dnmt1s-specific antibody UPT82 (Ratnam et al., 2002) (data not shown). Dnmt1s was also detected in morula-stage embryos by both N48 and UPT82 antibodies (data not shown).

To determine the localization of Dnmt1s, MII-stage unfertilized oocytes were stained with the N48 antibody. In contrast to the cytoplasmic distribution of Dnmt1o as shown by staining with H-300, Dnmt1s signals were exclusively localized to meiotic chromosomes (Fig. 1C). After fertilization, growing preimplantation embryos showed the presence of Dnmt1s in the nucleus until the blastocyst stage, whereas Dnmt1o signals were predominantly detected in the cytoplasm (Fig. 1D). Although previous reports showed nuclear translocation of Dnmt1o at the 8-cell stage (Doherty et al., 2002; Howell et al., 2001), H-300 antibody detected only weakly the nuclear Dnmt1o possibly due to differences in epitope recognition. These results indicate that Dnmt1s proteins are translated and localized to the nucleus during preimplantation development, whereas Dnmt1o reciprocally distributes throughout the cytoplasm.

Differential localization of Dnmt1s between paternal and maternal pronuclei

To investigate the dynamics of Dnmt1s localization from fertilization to the first cleavage, mouse one-cell embryos were collected 2 and 5 h after intracytoplasmic sperm injection (ICSI), and 21, 27 and 30 h after hCG injection with natural crossbreeding. Embryos were then stained with N48 antibody and propidium iodide (PI). According to the size and location of the pronuclei in the cytoplasm, samples were assigned to one of the pronuclear stages, PN0–PN5 (Adenot et al., 1997; Santos et al., 2002). Each sampling time approximately corresponded to PN0, PN1–2, PN3–4, PN5 and M-phase, respectively.
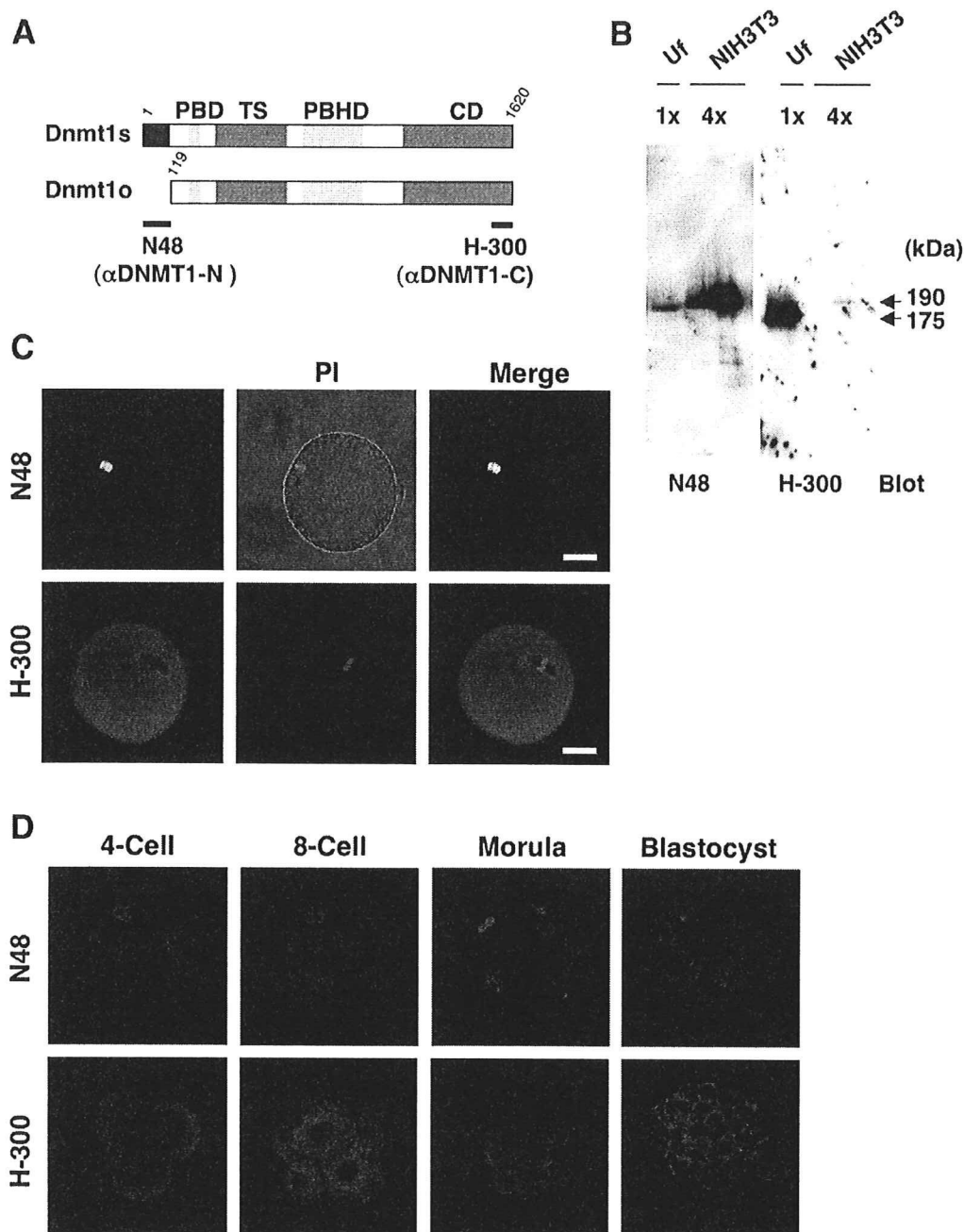
Fig. 1. Presence and localization of Dnmt1s in mouse unfertilized eggs and preimplantation embryos. (A) Structures of Dnmt1 isoforms and locations of epitopes recognized by two different antibodies; N48 and H-300. PBD, PCNA binding domain; TS, DNA replication foci-targeting sequence; PBHD, polybromo homology domain; CD, catalytic domain. (B) Western blotting of extracts from mouse unfertilized eggs (Uf) and NIH3T3 cells, probed with N48 and then reprobed with H-300. N48 detected only the 190 kDa Dnmt1s, whereas H-300 detected both 190 kDa Dnmt1s and 175 kDa Dnmt1o. Signals from different volumes (1× and 4×) of NIH3T3 extracts were used for comparison of relative amounts of Dnmt1 isoforms. (C) Immunostaining of mouse MII-stage unfertilized eggs with N48 and H-300. DNA was visualized by PI staining. For staining with N48 and PI, the PI staining image was superimposed on the corresponding light microscopic image. Dnmt1s colocalizes with meiotic chromosomes, as seen in yellow (merged image), whereas Dnmt1o distributes reciprocally in the cytoplasm. Scale bars indicate 20 μm. (D) Immunostaining of mouse preimplantation embryos. Dnmt1s is detected in the nuclei, whereas Dnmt1o is predominantly distributed in the cytoplasm.

At PN0, the fertilizing sperm is decondensed and the second polar body is eliminated upon the completion of meiosis. At this stage, Dnmt1s was exclusively detected in association with the maternal genome (Fig. 2A). As maturation of the pronuclei proceeded from PN1 to PN4, faint Dnmt1s signals also appeared in the paternal pronucleus, although at lower intensity than that of the maternal pronucleus (Figs. 2B, C). In three embryos at PN3–4, intense Dnmt1s signals were detected in the paternal pronucleus in a punctate pattern (Fig. 2D). These findings indicate that Dnmt1s is recruited to the paternal
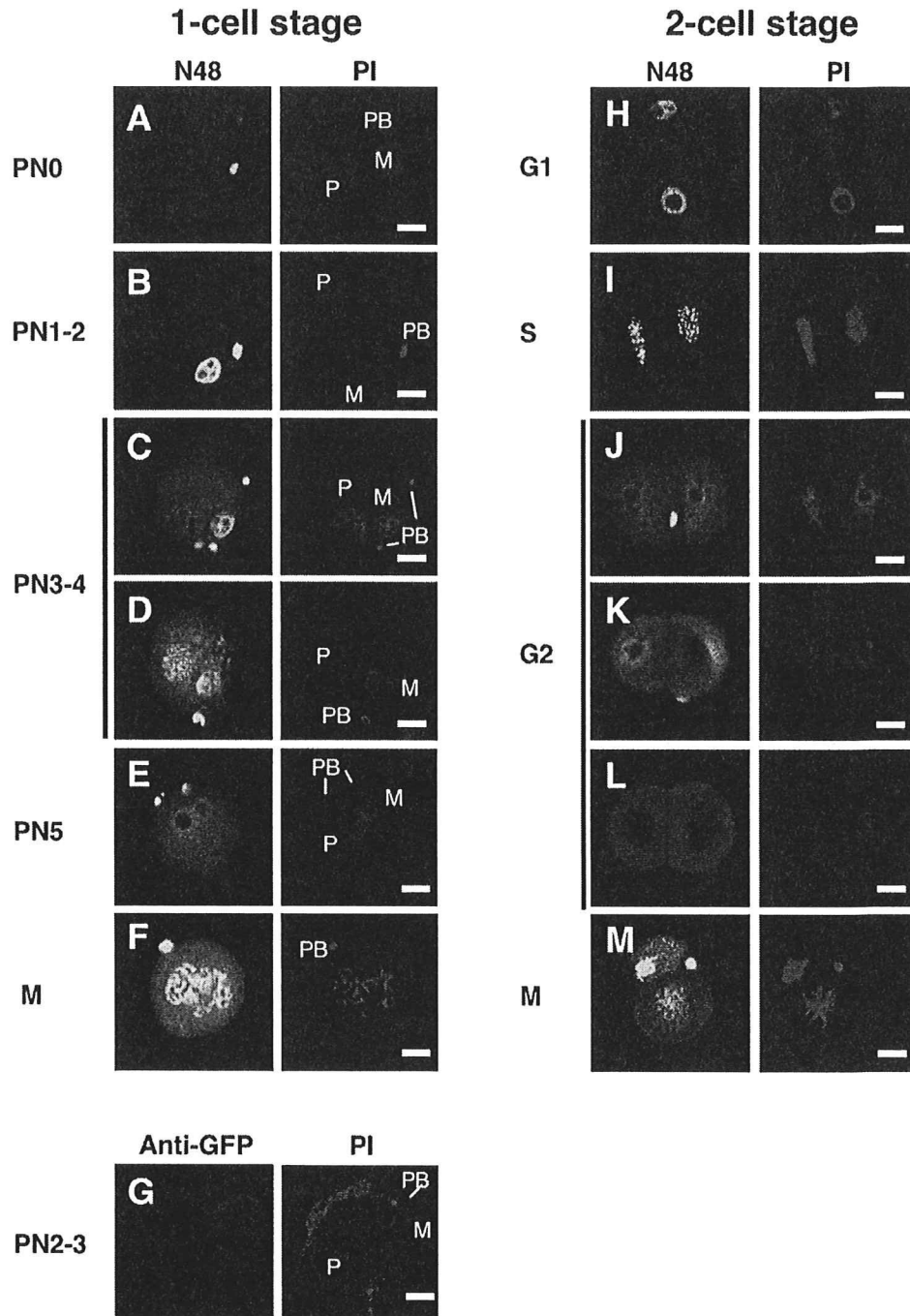
Fig. 2. Localization of Dnmt1s in one- and two-cell stage embryos. (A–F) Representative immunofluorescent images of one-cell embryos stained with the N48 antibody at different pronuclear stages. DNA was visualized by PI staining. The identity of the pronuclei was determined by their size and position relative to the polar body. At PN0, Dnmt1s is detected only in association with the maternal genome (A). Dnmt1s is thereafter localized predominantly in the maternal pronucleus until PN5 (B–D). Dnmt1 is also detected in the paternal nucleus, but the signals are quite faint (B, C). At PN3–4, some embryos show intense Dnmt1s signals in the paternal pronucleus in a punctate pattern (D). At PN5, Dnmt1s largely disappears from the pronuclei (E). At syngamy, Dnmt1 again colocalizes to the chromosome (F). (G) Control staining with anti-GFP antibody. (H–M) Representative immunofluorescent images of two-cell embryos stained with the N48 antibody at different cell cycle phases. Dnmt1 localizes in the nucleus through the G1 (H) to the S phase (I). Dnmt1s signals in the S phase show a punctate pattern. Then, Dnmt1s in the nucleus was largely decreased in the G2 phase (J). In some cases, Dnmt1s signals were absent from the nucleus in either (K) or both (L) of the blastomeres in G2. In the M phase, Dnmt1 again localizes in close association with the chromosomes (M). M, maternal pronucleus; P, paternal pronucleus; PB, polar body. Scale bars indicate 20 μm.

genome during pronuclear maturation with a peak during PN3–4. At PN5, Dnmt1s signals in the maternal pronucleus were reduced to the paternal pronucleus level (Fig. 2E). During mitosis, Dnmt1s again colocalized intensely to the chromosomes (Fig. 2F). Staining with anti-GFP antibody as negative control gave little signals (Fig. 2G).

Dynamic changes in nuclear localization of Dnmt1s in early preimplantation embryos

In addition to asymmetric localization of Dnmt1s in the pronuclei, immunostaining analysis revealed dynamic changes in this protein during pronuclear maturation through to the first cleavage. The pronuclear staging has been shown to correlate with cell cycle phases; PN1–2 embryos are in G1, PN3–4 embryos are largely in S, and PN5 embryos are mostly in G2 (Adenot et al., 1997). Significantly, the punctate pattern of Dnmt1s signals in PN3–4 embryos is very similar to that associated with the DNA replication foci in cultured somatic cells in middle and late S phase (Leonhardt et al., 1992; Liu et al.,

1998). Therefore, the dynamics of localization in one-cell embryos suggest that Dnmt1 may be recruited and sustained in the pronucleus during the G1 to S phases, and then excluded from the pronucleus in the G2 phase. To test this possibility at later stages, we examined the dynamics of Dnmt1s localization in two-cell embryos.

It has been reported that, during the second cell cycle, the G1, S and G2 phases last about 2, 6–7 and 14 h, respectively (Moore et al., 1996). On the basis of this report, two-cell embryos were collected 1 h (G1), 6 h (S) and 12–20 h (G2) after the first cleavage and stained with N48 antibody and PI. Dnmt1s was diffusely distributed in the nucleoplasm in the G1 phase (Fig. 2H). In the S phase, Dnmt1s signals showed a punctate pattern in the nucleus (Fig. 2I), as seen in somatic cells in the same phase. In contrast, many embryos exhibited significantly reduced Dnmt1s signals in the nucleus during the G2 phase (Fig. 2J). In some cases, Dnmt1s signals were absent from the nucleus in either or both of the blastomeres (Figs. 2K, L), indicating the transient disappearance of Dnmt1s from the nucleus during the G2 phase. During mitosis, Dnmt1s was
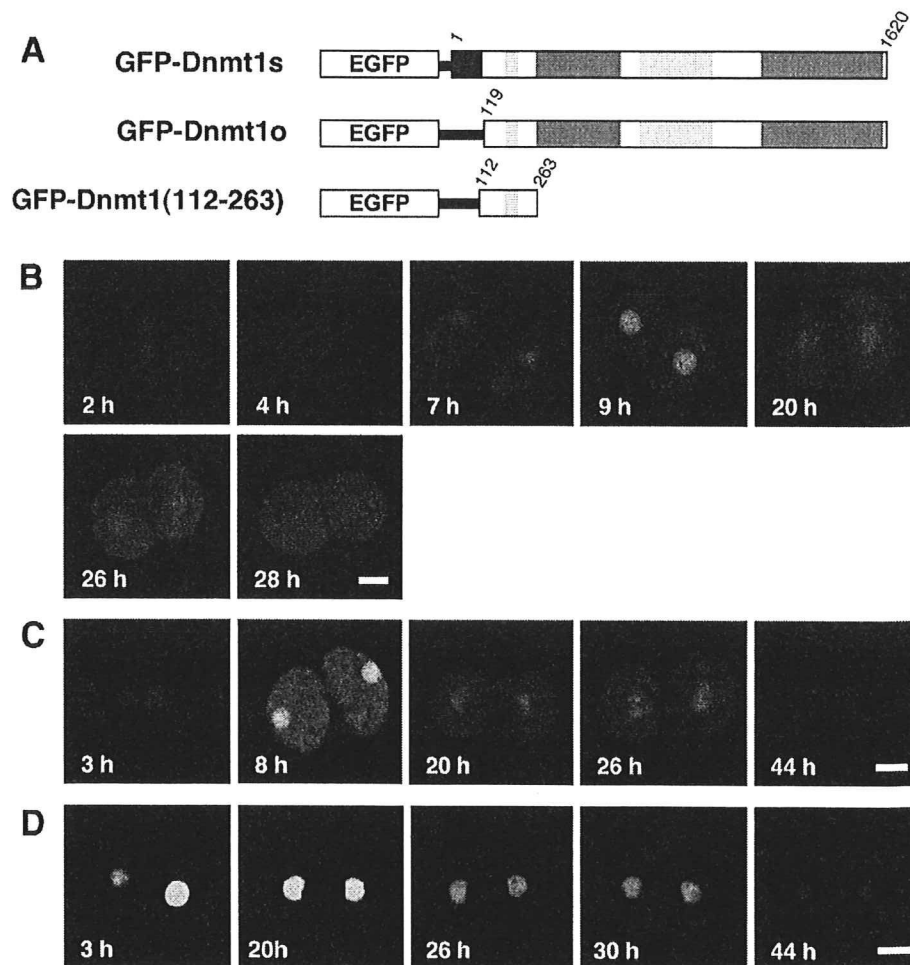

Fig. 3. Dynamic changes in the localization of EGFP-Dnmt1 mutant proteins. (A) Structures of EGFP-Dnmt1 mutant proteins. (B–D) *In vitro* transcripts for EGFP-Dnmt1s (B), EGFP-Dnmt1o (C) and EGFP-Dnmt1(112–263) (D) were microinjected into one-cell embryos and fluorescent images were serially obtained by confocal microscopy. Shown are representative embryos expressing each EGFP-Dnmt1 mutant protein. Time is in hours after mRNA injection. Scale bars indicate 20 μm.
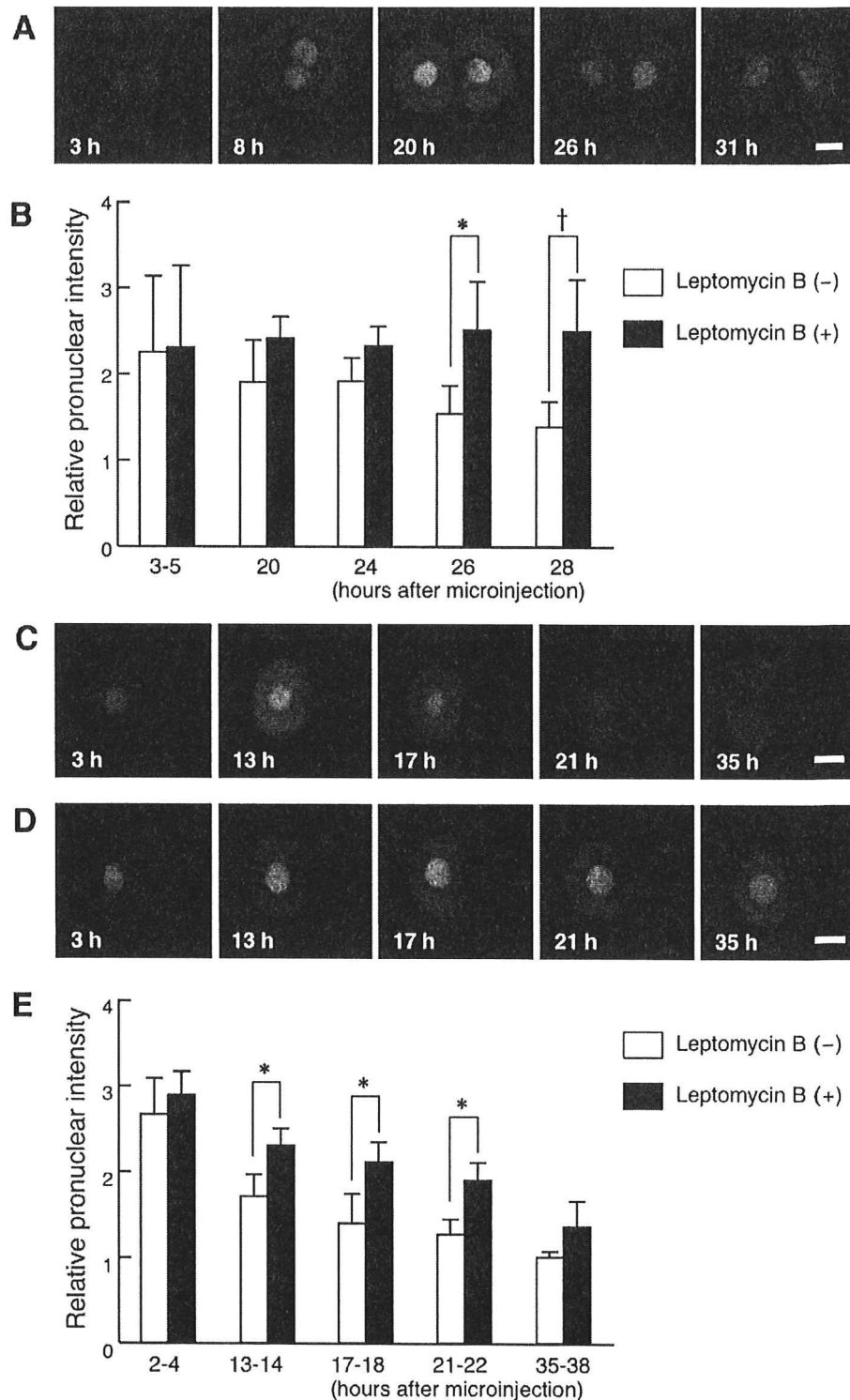
Fig. 4. Effects of leptomycin B on the dynamics of EGFP-Dnmt1s localization. (A) *In vitro* transcripts for EGFP-Dnmt1s were microinjected into one-cell embryos. Embryos were then cultured in the presence of leptomycin B. Fluorescent images were serially obtained by confocal microscopy. Time is in hours after mRNA injection. Scale bars indicate 20 μm. (B) Comparison of the relative nuclear intensity of EGFP-Dnmt1s signals after mRNA injection into one-cell embryos in the absence (open columns) and presence (filled columns) of leptomycin B. The columns and bars represent means±S.D. of 4–6 measurements per data point. *$P < 0.05$, †$P < 0.01$. (C, D) *In vitro* transcripts for EGFP-Dnmt1s were microinjected into one-half of two-cell embryos. Embryos were then cultured in the absence (C) and presence (D) of leptomycin B. Fluorescent images were serially obtained by confocal microscopy. Time is in hours after mRNA injection. Scale bars indicate 20 μm. (E) Comparison of the relative nuclear intensity of EGFP-Dnmt1s signals after mRNA injection into one-half of two-cell embryos in the absence (open columns) and presence (filled columns) of leptomycin B. The columns and bars represent means±S.D. of 4–6 measurements per data point. *$P < 0.005$.

detected around the mitotic chromosomes, although the signals did not completely coincide with the chromosomes (Fig. 2M).

Nuclear-cytoplasmic shuttling of GFP-Dnmt1s in early preimplantation embryos

To confirm the dynamics of nuclear Dnmt1s localization and clarify the underlying mechanism, we constructed plasmids encoding fusion proteins of EGFP with full-length Dnmt1s or

its mutants (Fig. 3A), and injected their *in vitro* transcripts into early stage embryos. When EGFP-Dnmt1s mRNA was injected into ~200 one-cell embryos 24–26 h after hCG injection, 36 embryos showed EGFP signals in their pronuclei 1–2 h after injection and 11 embryos reached the two-cell stage with nuclear EGFP signals. Disappearance of EGFP-Dnmt1s from the pronuclei at PN5 could be verified in 8 of the 11 embryos (Fig. 3B). At the two-cell stage, EGFP signals were again localized to the nucleus within several hours after the first
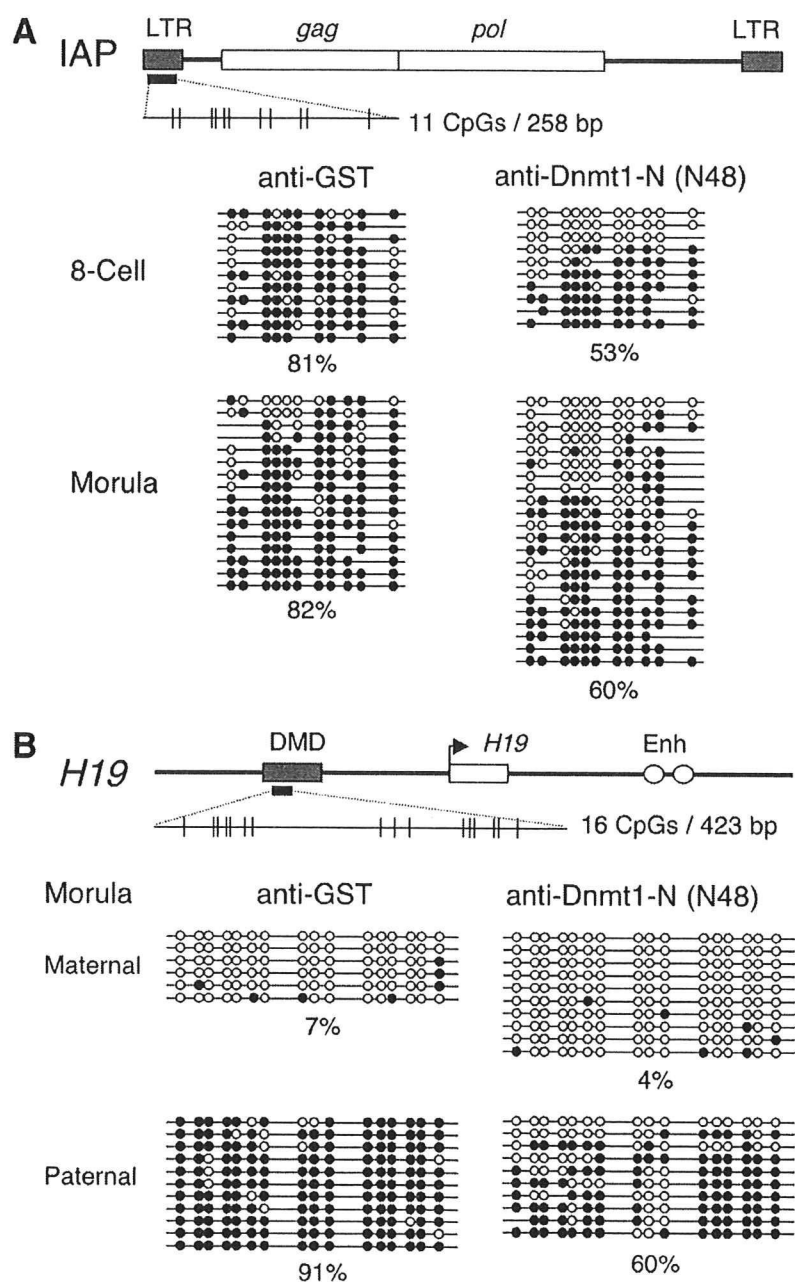

Fig. 5. Effects of antibody microinjection on DNA methylation states in preimplantation embryos. (A) Bisulfite sequencing profiles of the LTR of IAP in antibody-injected embryos at the eight-cell and morula stages. (B) Bisulfite sequencing profiles of the DMD of the paternal *H19* allele in antibody-injected embryos at the morula stage. Open and filled circles represent unmethylated and methylated CpGs, respectively. Each line corresponds to an individual DNA strand. The overall percentage of methylated CpGs is shown below each group of clones.

cleavage, but had mostly disappeared from the nucleus around the G2 phase (Fig. 3B), mimicking the behavior of Dnmt1s-immunoreactivity in embryos at the same stage. When EGFP-Dnmt1o mRNA was injected into one-cell embryos, EGFP-Dnmt1o protein was also localized to the nucleus as in case of EGFP-Dnmt1s (Fig. 3C). In contrast, EGFP-fusion protein with the N-terminal region containing putative nuclear localization signals (amino acids 112–263) resulted in retention of EGFP signals in the nucleus (Fig. 3D). These results indicate that the disappearance of Dnmt1 from the (pro)nucleus is not due to the presence of EGFP and does not require the Dnmt1s-specific N-terminal region.

To test whether the decrease in nuclear EGFP signals was attributable to active nuclear export, embryos were injected with EGFP-Dnmt1s mRNA at the one-cell stage and then treated with leptomycin B, an inhibitor of CRM1/exportin-mediated nuclear export. EGFP signals were retained in the nucleus with high intensity in leptomycin B-treated embryos (Figs. 4A, B). EGFP-Dnmt1s mRNA was also injected into one-half of two-cell embryos 1–4 h after the first cleavage. Among ∼220 embryos injected, 22 expressed EGFP-Dnmt1s protein in the injected half. In all seven embryos that grew to the four-cell stage within 36 h after the first cleavage, nuclear EGFP-Dnm1s signals were largely suppressed during the G2 phase, whereas cytoplasmic EGFP signals were sustained (Fig. 4C). In the presence of leptomycin B, however, EGFP signals were retained in the nucleus with high intensity (Fig. 4D). These results indicate that the decrease in nuclear EGFP-Dnmt1s
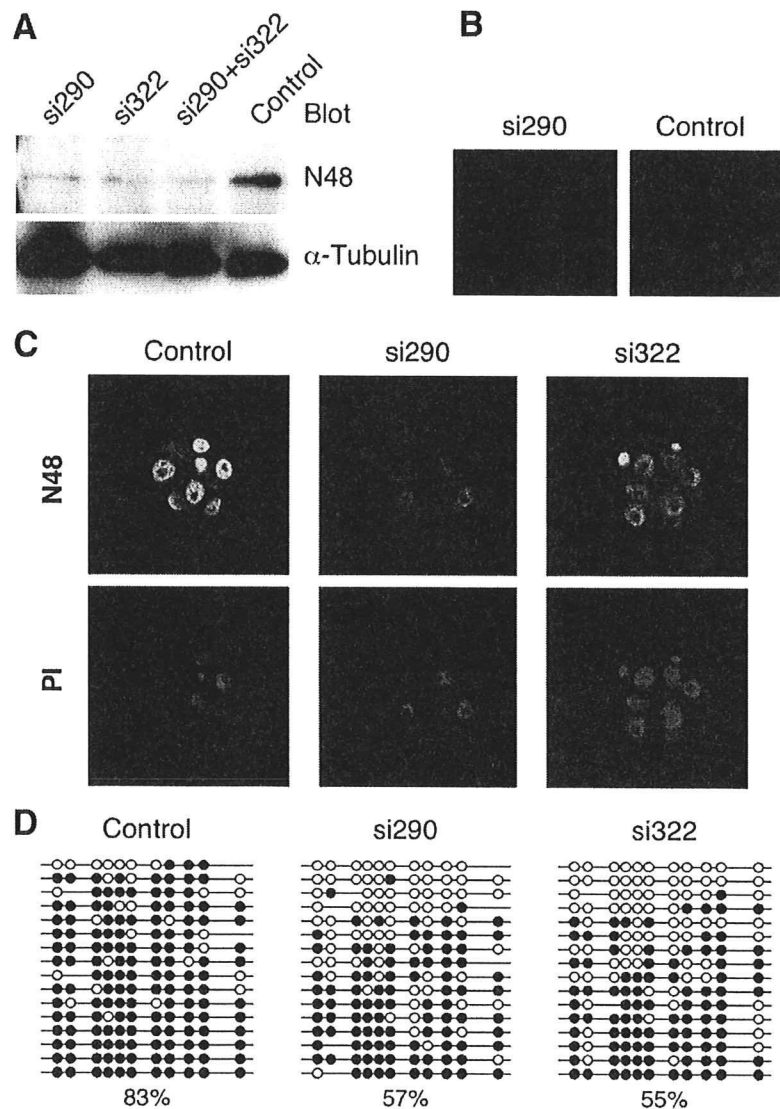

Fig. 6. Effects of Dnmt1-targeted siRNA microinjection on DNA methylation states in preimplantation embryos. (A, B) Efficient downregulation of Dnmt1s protein by siRNA was verified in NIH 3T3 cells by Western blotting (A) and immunostaining (B) with N48 antibody. (C) Immunostaining analysis of 8–16 cell embryos injected with control and Dnmt1 siRNA, probed with the N48 antibody. DNA was counterstained with PI. Dnmt1 expression is effectively knocked-down in Dnmt1 siRNA-injected embryos. (D) Bisulfite sequencing profiles of the IAP LTRs in siRNA-injected embryos at the morula stage. Open and filled circles represent unmethylated and methylated CpGs, respectively. Each line corresponds to an individual DNA strand. The overall percentage of methylated CpGs is shown below each group of clones.

during the G2 phase is attributable to CRM1/exportin-dependent nuclear export.

Microinjection of anti-Dnmt1 antibody affects DNA methylation patterns

To examine whether Dnmt1s present in preimplantation embryos is responsible for the maintenance of DNA methylation during this stage, we evaluated genomic methylation patterns using two different approaches. First, we performed ICSI with co-injection of N48, expecting that it might function as a Dnmt1s-specific neutralizing antibody. In control embryos injected with anti-GST antibody, the long terminal repeats (LTR) of IAPs were highly methylated as revealed by bisulfite sequencing at the eight-cell and morula stages (81% and 82%, respectively) (Fig. 5A). Injection with N48 antibody resulted in a significant decrease in DNA methylation of IAPs at the morula stage (60%, $P<0.05$) (Fig. 5A). Similar phenomenon was observed at the 8-cell stage, although it was not statistically significant (53%, $P=0.064$) (Fig. 5A). Notably, some IAP sequences showed complete or nearly-complete demethylation in N48-injected embryos, which was consistent with the failure of DNA methylation maintenance (Fig. 5A). We also analyzed the effect of N48 injection on the methylation state of the paternally imprinted *H19* gene. To determine the parental origins of alleles, we injected sperm from *M. m. castaneus* males into oocytes from ICR females with N48 or control anti-GST antibodies. In embryos injected with control antibody, the differentially methylated domain (DMD) of the *H19* gene of the paternal allele was highly methylated at the morula stage (91%), whereas that of the maternal allele was mostly demethylated (7%) (Fig. 5B). In N48-injected embryos, the percentage of DNA methylation in this region of the paternal allele was significantly decreased (60%, $P<0.01$), whereas that of the maternal allele was similarly demethylated (4%) (Fig. 5B). These results indicate the methylated CpGs dinucleotides in the IAP and *H19* gene loci to be decreased by microinjection of anti-Dnmt1s antibody.

Dnmt1-targeted siRNA affects DNA methylation patterns

To further investigate the role of Dnmt1s in maintenance methylation, we adopted RNAi-mediated knock-down experiments because Dnmt1s, rather than Dnmt1o, is known to be actively transcribed during preimplantation development (Ratnam et al., 2002 and our unpublished data). siRNA was designed to target against Dnmt1s mRNA and tested in NIH 3T3 cells. Western blotting (Fig. 6A) and immunostaining with N48 antibody (Fig. 6B) confirmed the effectiveness of the siRNA. We then injected Dnmt1s siRNA duplexes into fertilized eggs at the pronuclear stage and analyzed their effects on the methylation state of IAPs to test whether the decrease in DNA methylation induced by antibody injection could be reproduced by RNAi-mediated Dnmt1s knock-down. Two independent siRNAs, si290 and si322, against Dnmt1s down-regulated Dnmt1s expression also in preimplantation embryos, as revealed by immunostaining (Fig. 6C). Microinjection of

either Dnmt1s siRNA resulted in significant decreases in DNA methylation of IAPs at the morula stages (57% and 55%, $P<0.05$ for si290 and si322, respectively), as compared with that of embryos injected with a control siRNA (83%) (Fig. 6D). As in N48-injected embryos, some IAP sequences demonstrated complete or nearly-complete demethylation (Fig. 6D). Taken together, these results indicate that Dnmt1s synthesized after fertilization is involved in the maintenance methylation of certain repetitive sequences and imprinted genes.

Discussion

Fertilization initiates epigenetic reprogramming to establish totipotency in the early embryo. Large part of the gametic genome undergoes active or passive DNA demethylation and chromatin remodeling into a zygotic pattern. In contrast, the methylation states of some genomic regions including repetitive sequences and imprinted genes are faithfully maintained during the same period. Failure to identify the enzyme(s) responsible for maintenance DNA methylation in the nucleus of preimplantation embryos, expect for Dnmt1o at the eight-cell stage, has hampered the clarification of mechanisms by which the genomic sequences are selected for demethylation or maintenance methylation and epigenetic reprogramming proceeds precisely.

In the present study, we demonstrated the presence of Dnmt1s protein in the nuclei of preimplantation embryos. This finding is quite contrary to previous literature demonstrating that no Dnmt1s protein is translated from its mRNA during this period. Very low amounts of Dnmt1s relative to cytoplasmic Dnmt1o may have prevented it from detection. Especially, the UPT82 antibody, which can recognize the Dnmt1s-specific N-terminal region, has been reported to detect Dnmt1s in preimplantation embryos when Dnmt1s is forcedly expressed in oocytes (Ratnam et al., 2002), and in 4-,8- and 16-cell embryos that are missing Dnmt1o (Chung et al., 2003). In the later case, loss of Dnmt1o is assumed to cause aberrant expression of Dnmt1s. This apparent discrepancy may be due to differences in sensitivity of antibodies and/or epitope sites to be recognized, which might be protected from recognition by posttranslational modification or complex formation. Indeed, it has been reported that an antibody which recognizes the Dnmt1s-specific N-terminal region could detect Dnmt1s protein in association with mitotic chromatin in somatic cells, while other antibodies could not detect it (Easwaran et al., 2004), indicating the detectability of Dnmt1s may be context-dependent even in the same cells.

Asymmetric distribution of Dnmt1s in the parental genome may be linked to differential reprogramming processes after fertilization. Upon fertilization, the paternal genome undergoes extensive demethylation before the initiation of DNA replication, whereas the maternal genome is protected from this active demethylation and completes the second meiosis. Although the mechanism of active demethylation remains unknown, epigenetic differences between gametes at fertilization are thought to contribute to the establishment of this parental asymmetry (Morgan et al., 2005). The presence of Dnmt1s, together with

high contents of methylated histone H3 and heterochromatin proteins such as HP1β, may protect the maternal genome from active demethylation. On the other hand, Dnmt1s is absent from decondensing sperm and is gradually recruited to the paternal genome during the first cell cycle. This time course is similar to those of some epigenetic changes such as K9 dimethylation and K27 trimethylation of histone H3 (Morgan et al., 2005; Santos et al., 2005). Di/trimethylated H3-K9 and trimethylated H3-K27 are specifically targeted by the chromodomains of HP1 and polycomb proteins, respectively (Margueron et al., 2005). In fact, HP1β is also recruited to the paternal genome during a similar period (Santos et al., 2005). Because HP1β and its interacting partner SUV39H1 can associate with Dnmt1 (Fuks et al., 2003), these factors may mediate the recruitment of Dnmt1s to the paternal genome and cooperate with it in reestablishing an epigenetic state equivalent to the maternal one.

Immunostaining demonstrates cell cycle-coupled dynamics of Dnmt1s localization during at least the first two cell cycles. The effect of leptomycin B on Dnmt1s localization indicates that nuclear Dnmt1s appears to translocate to the cytoplasm in the G2 phase via CRM1/exportin-mediated nuclear export. This phenomenon may be highly characteristic of preimplantation embryos at this stage, because endogenous and forcedly-expressed Dnmt1s is localized in the nucleus throughout cell cycle in somatic cells such as NIH3T3 cells and HeLa cells (Easwaran et al., 2004, and our unpublished data). Dnmt1 contains a leucine-rich region in its C-terminus, which is close to the consensus sequence of the nuclear export signal (NES), which is recognized by CRM1/exportin (Kutay and Guttinger, 2005). This region may act as a functional NES in the G2 phase of preimplantation embryos.

Interestingly, EGFP-Dnmt1o was also localized to the nucleus and thereafter translocated to the cytoplasm. We speculate that the initial localization to the nucleus and translocation to the cytoplasm thereafter do not require the Dnmt1s-specific N-terminal region. It also raises a possibility that *de novo*-synthesized Dnmt1o may first localize to the nucleus and may be thereafter sequestered to the cytoplasm by an active mechanism. It has been previously reported that Dnmt1o interacts and colocalizes with annexin V (Ohsawa et al., 1996), a calcium-sensitive phospholipid binding protein (Schlaepfer et al., 1987). This interaction is postulated to lead to active sequestration of Dnmt1o in the cytoplasm of unfertilized oocytes and preimplantation embryos (Doherty et al., 2002). This may explain the difference in subcellular localization between Dnmt1s and Dnmt1o.

At present, there is no evidence supporting the relation between this phenomenon and genome-wide demethylation. However, it might be possible that the disappearance of Dnmt1s from the nucleus in G2 decreases the opportunity for this enzyme to be recruited to hemi-methylated CpG regions or nuclear complexes containing proteins interactive with it after the S phase. Indeed, previous reports have demonstrated that Dnmt1s associates with chromatin (preferentially constitutive heterochromatin) during the G2 and M phases through a mechanism different from a replication dependent one in the S phase (Easwaran et al., 2004). Thus, the depletion of nuclear Dnmt1s in G2 may be related to the limited maintenance methylation during preimplantation development.

Decreases in methylated CpG dinucleotides in the LTR of IAPs and the paternal allele of *H19* in response to microinjection of N48 or Dnmt1 siRNA suggest nuclear-localized Dnmt1s to be involved in maintenance methylation during preimplantation development. The presence of Dnmt1s in the nucleus and its function in maintenance methylation appear to compensate for the limited role of Dnmt1o, which apparently translocates to the nucleus only at the eight-cell stage (Howell et al., 2001), during preimplantation development. In preimplantation embryos, methylation states are maintained only in limited genomic sequences, in contrast to the situation in somatic cells. Taken together with the observation that the localization of Dnmt1s fluctuates via nucleocytoplasmic shuttling in preimplantation embryos, these findings indicate that this characteristic behavior of Dnmt1s may restrict its recruitment to certain genomic regions, allowing large portions of the genomic DNA to be demethylated. The mechanism by which Dnmt1s is recruited to particular regions in the ubiquitously methylated genome of preimplantation embryos should be further investigated.

In the present study, about 50% to 60% of CpG dinucleotides in the LTR of IAPs and the paternal allele of *H19* remained methylated after microinjection of N48 or Dnmt1 siRNA. This partial demethylation may be due to the presence of Dnmt1o and/or incomplete inactivation of Dnmt1s with the methods used in this study. In our preliminary experiment, however, embryos injected with Dnmt1 siRNA tended to show growth retardation after implantation, as compared to control siRNA-injected embryos (data not shown). This result may support the idea that Dnmt1s activity in preimplantation embryos is required for normal postimplantation development, although it may also be possible that the effect of injected siRNA was retained after implantation to affect the growth thereafter.

Recently, Sasaki's group established oocyte-specific Dnmt1 knockout mice and demonstrated that Dnmt1, but not Dnmt3a and 3b, is mostly responsible for maintenance DNA methylation during preimplantation development (Ryutaro Hirasawa and Hiroyuki Sasaki, personal communication). Taken together with only partial reduction in DNA methylation in Dnmt1o-specific knockout embryos reported previously (Howell et al., 2001), their results are consistent with us in that Dnmt1s may compensate the absence of Dnmt1o in the nucleus except for the 8-cell stage during preimplantation development. Dnmt1s-specific gene knockout is expected to further clarify this issue.

In conclusion, the present study has revealed the presence of Dnmt1s in the nucleus and its nucleocytoplasmic shuttling in preimplantation embryos. Inactivation of Dnmt1s by microinjection of Dnmt1s-specific antibody and siRNA resulted in decreases of methylated CpG dinucleotides in the genomic regions whose methylation patterns must be maintained after fertilization. These findings may contribute to the understanding of the mechanism underlying epigenetic regulation during preimplantation development.

Acknowledgments

References

Adenot, P.G., Mercier, Y., Renard, J.P., Thompson, E.M., 1997. Differential H4 acetylation of paternal and maternal chromatin precedes DNA replication and differential transcriptional activity in pronuclei of 1-cell mouse embryos. Dev. Biol. 124, 4615–4625.

Aida, T., Oda, S., Awaji, T., Yoshida, K., Miyazaki, S., 2001. Expression of a green fluorescent protein variant in mouse oocytes by injection of RNA with an added long poly(A) tail. Mol. Hum. Reprod. 7, 1039–1046.

Bestor, T.H., 2000. The DNA methyltransferases of mammals. Hum. Mol. Genet. 9, 2395–2402.

Bestor, T., Laudano, A., Mattaliano, R., Ingram, V., 1988. Cloning and sequencing of a cDNA encoding DNA methyltransferase of mouse cells. The carboxyl-terminal domain of the mammalian enzymes is related to bacterial restriction methyltransferases. J. Mol. Biol. 203, 971–983.

Cardoso, M.C., Leonhardt, H., 1999. DNA methyltransferase is actively retained in the cytoplasm during early development. J. Cell. Biol. 147, 25–32.

Chuang, L.S., Ian, H.I., Koh, T.W., Ng, H.H., Xu, G., Li, B.F., 1997. Human DNA-(cytosine-5) methyltransferase–PCNA complex as a target for p21WAF1. Science 277, 1996–2000.

Chung, Y.G., Ratnam, S., Chaillet, J.R., Latham, K.E., 2003. Abnormal regulation of DNA methyltransferase expression in cloned mouse embryos. Biol. Reprod. 69, 146–153.

Dean, W., Santos, F., Reik, W., 2003. Epigenetic reprogramming in early mammalian development and following somatic nuclear transfer. Semin. Cell Dev. Biol. 14, 93–100.

Doherty, A.S., Bartolomei, M.S., Schultz, R.M., 2002. Regulation of stage-specific nuclear translocation of Dnmt1o during preimplantation mouse development. Dev. Biol. 242, 255–266.

Easwaran, H.P., Schermelleh, L., Leonhardt, H., Cardoso, M.C., 2004. Replication-independent chromatin loading of Dnmt1 during G2 and M phases. EMBO Rep. 5, 1181–1186.

Egger, G., Liang, G., Aparicio, A., Jones, P.A., 2004. Epigenetics in human disease and prospects for epigenetic therapy. Nature 429, 457–463.

Fuks, F., Hurd, P.J., Deplus, R., Kouzarides, T., 2003. The DNA methyltransferases associate with HP1 and the SUV39H1 histone methyltransferase. Nucleic Acids Res. 31, 2305–2312.

Gaudet, F., Rideout III, W.M., Meissner, A., Dausman, J., Leonhardt, H., Jaenisch, R., 2004. Dnmt1 expression in pre- and postimplantation embryogenesis and the maintenance of IAP silencing. Mol. Cell. Biol. 24, 1640–1648.

Howell, C.Y., Bestor, T.H., Ding, F., Latham, K.E., Mertineit, C., Trasler, J.M., Chaillet, J.R., 2001. Genomic imprinting disrupted by a maternal effect mutation in the Dnmt1 gene. Cell 104, 829–838.

Jaenisch, R., Bird, A., 2003. Epigenetic regulation of gene expression: how the genome integrates intrinsic and environmental signals. Nat. Genet. 33, 245–254.

Kimura, Y., Yanagimachi, R., 1995. Intracytoplasmic sperm injection in the mouse. Biol. Reprod. 52, 709–720.

Kutay, U., Guttinger, S., 2005. Leucine-rich nuclear-export signals: born to be weak. Trends Cell Biol. 15, 121–124.

Lane, N., Dean, W., Erhardt, S., Hajkova, P., Surani, A., Walter, J., Reik, W., 2003. Resistance of IAPs to methylation reprogramming may provide a mechanism for epigenetic inheritance in the mouse. Genesis 35, 88–93.

Leonhardt, H., Page, A.W., Weier, H.U., Bestor, T.H., 1992. A targeting sequence directs DNA methyltransferase to sites of DNA replication in mammalian nuclei. Cell 71, 865–873.

Li, E., 2002. Chromatin modification and epigenetic reprogramming in mammalian development. Nat. Rev., Genet. 3, 662–673.

Li, E., Bestor, T.H., Jaenisch, R., 1992. Targeted mutation of the DNA methyltransferase gene results in embryonic lethality. Cell 69, 915–926.

Liu, Y., Oakeley, E.J., Sun, L., Jost, J.P., 1998. Multiple domains are involved in the targeting of the mouse DNA methyltransferase to the DNA replication foci. Nucleic Acids Res. 26, 1038–1045.

Margueron, R., Trojer, P., Reinberg, D., 2005. The key to development: interpreting the histone code? Curr. Opin. Genet. Dev. 15, 163–176.

Mayer, W., Niveleau, A., Walter, J., Fundele, R., Haaf, T., 2000. Demethylation of the zygotic paternal genome. Nature 403, 501–502.

Mertineit, C., Yoder, J.A., Taketo, T., Laird, D.W., Trasler, J.M., Bestor, T.H., 1998. Sex-specific exons control DNA methyltransferase in mammalian germ cells. Dev. Biol. 125, 889–897.

Moore, G.D., Ayabe, T., Kopf, G.S., Schultz, R.M., 1996. Temporal patterns of gene expression of G1-S cyclins and cdks during the first and second mitotic cell cycles in mouse embryos. Mol. Reprod. Dev. 45, 264–275.

Morgan, H.D., Santos, F., Green, K., Dean, W., Reik, W., 2005. Epigenetic reprogramming in mammals. Hum. Mol. Genet. 14 (Spec No. 1), R47–R58.

Ohsawa, K., Imai, Y., Ito, D., Kohsaka, S., 1996. Molecular cloning and characterization of annexin V-binding proteins with highly hydrophilic peptide structure. J. Neurochem. 67, 89–97.

Okano, M., Xie, S., Li, E., 1998. Cloning and characterization of a family of novel mammalian DNA (cytosine-5) methyltransferases. Nat. Genet. 19, 219–220.

Okano, M., Bell, D.W., Haber, D.A., Li, E., 1999. DNA methyltransferases Dnmt3a and Dnmt3b are essential for de novo methylation and mammalian development. Cell 99, 247–257.

Olek, A., Oswald, J., Walter, J., 1996. A modified and improved method for bisulphite based cytosine methylation analysis. Nucleic Acids Res. 24, 5064–5066.

Oswald, J., Engemann, S., Lane, N., Mayer, W., Olek, A., Fundele, R., Dean, W., Reik, W., Walter, J., 2000. Active demethylation of the paternal genome in the mouse zygote. Curr. Biol. 10, 475–478.

Ratnam, S., Mertineit, C., Ding, F., Howell, C.Y., Clarke, H.J., Bestor, T.H., Chaillet, J.R., Trasler, J.M., 2002. Dynamics of Dnmt1 methyltransferase expression and intracellular localization during oogenesis and preimplantation development. Dev. Biol. 245, 304–314.

Reik, W., Dean, W., Walter, J., 2001. Epigenetic reprogramming in mammalian development. Science 293, 1089–1093.

Rougier, N., Bourc'his, D., Gomes, D.M., Niveleau, A., Plachot, M., Paldi, A., Viegas-Pequignot, E., 1998. Chromosome methylation patterns during mammalian preimplantation development. Genes Dev. 12, 2108–2113.

Santos, F., Dean, W., 2004. Epigenetic reprogramming during early development in mammals. Reproduction 127, 643–651.

Santos, F., Hendrich, B., Reik, W., Dean, W., 2002. Dynamic reprogramming of DNA methylation in the early mouse embryo. Dev. Biol. 241, 172–182.

Santos, F., Peters, A.H., Otte, A.P., Reik, W., Dean, W., 2005. Dynamic chromatin modifications characterise the first cell cycle in mouse embryos. Dev. Biol. 280, 225–236.

Schlaepfer, D.D., Mehlman, T., Burgess, W.H., Haigler, H.T., 1987. Structural and functional characterization of endonexin II, a calcium- and phospholipid-binding protein. Proc. Natl. Acad. Sci. U. S. A. 84, 6078–6082.

Tremblay, K.D., Duran, K.L., Bartolomei, M.S., 1997. A 5′ 2-kilobase-pair region of the imprinted mouse H19 gene exhibits exclusive paternal methylation throughout development. Mol. Cell. Biol. 17, 4322–4329.

Warnecke, P.M., Mann, J.R., Frommer, M., Clark, S.J., 1998. Bisulfite sequencing in preimplantation embryos: DNA methylation profile of the upstream region of the mouse imprinted H19 gene. Genomics 51, 182–190.

Yoder, J.A., Walsh, C.P., Bestor, T.H., 1997. Cytosine methylation and the ecology of intragenomic parasites. Trends Genet. 13, 335–340.

SH3 domain of the phosphatidylinositol 3-kinase regulatory subunit is responsible for the formation of a sequestration complex with insulin receptor substrate-1

Yuichi Ikegami [a], Kouichi Inukai [a,*], Takuya Awata [a], Tomoichiro Asano [b], Shigehiro Katayama [a]

[a] *Division of Endocrinology and Diabetes, Department of Medicine, Saitama Medical University, Morohongo 38, Moroyama, Iruma-gun, Saitama 350-0495, Japan*
[b] *Division of Molecular Medical Science, Graduate School of Biomedical Sciences, Hiroshima University, Hiroshima, Japan*

Abstract

Class IA phosphatidylinositol 3-kinase (PI 3-kinase), which is composed of a 110 kDa catalytic subunit and a regulatory subunit, plays a key role in most insulin dependent cellular responses. To date, five mammalian regulatory subunit isoforms have been identified, including two 85 kDa proteins (p85α and p85β), two 55 kDa proteins (p55γ and p55α), and one 50 kDa protein (p50α). In the present study, we overexpressed these recombinant proteins, tagged with green fluorescent proteins (GFP), in CHO-IR cells and investigated intracellular localizations in both the presence and the absence of insulin stimulation. Interestingly, in response to insulin, only p85α and p85β redistributed to isolated foci in the cells, while both were present throughout the cytoplasm in quiescent cells. In contrast, p55s accumulated in the perinuclear region irrespective of insulin stimulation, while p50α behaved similarly to control GFP. Immuno-fluorescent antibodies against endogenous IRS-1 revealed IRS-1 to be co-localized in the p85 foci in response to insulin. As both insulin receptors and p110α catalytic subunits were absent from these foci on immunofluorescence study, only p85 and IRS-1 were suggested to form a sequestration complex in response to insulin. To determine the domain responsible for IRS-1 complex formation, we prepared and overexpressed the SH3 domain deletion mutant of p85α in CHO-IR cells. This mutant failed to form foci, suggesting the SH3 domain of regulatory subunits to be responsible for formation of the p85-IRS-1 sequestration complex. In conclusion, our study revealed the SH3 domain of PI 3-kinase to play a critical role in intracellular localizations, including formation of foci with IRS-1 in response to insulin.
© 2007 Elsevier Inc. All rights reserved.

Keywords: PI-3kinase; CHO-IR cells; IRS-1; Insulin; Akt

Class IA phosphatidylinositol 3-kinase (PI 3-kinase), which is composed of a catalytic 110 kDa protein (p110) associated with a regulatory subunit, has been implicated in the regulation of various cellular response activities, including proliferation, differentiation, membrane ruffling, prevention of apoptosis, and insulin stimulated glucose uptake [1–5]. The SH2 domain of the regulatory subunit

has been shown to bind directly to the tyrosine-phosphorylated YXXM motif of several activated receptor tyrosine kinases [6]. To date, five mammalian regulatory subunit isoforms have been identified, including two 85 kDa proteins (p85α and p85β), two 55 kDa proteins (p55γ and p55α), and one 50 kDa protein (p50α). All five isoforms share two SH2 domains but have different NH2-terminal sequences. The most well known 85 kDa isoforms contain SH3 and bcr homology (BH) domains in their N-termini [7]. The recently cloned 55 kDa isoforms contain a unique 34 amino acid sequence in their N-termini [8,9]. The

50 kDa isoform contains only a six amino acid sequence in its N-terminal portion, which is apparently too short to interact with other molecules [10].

In this study, we overexpressed these recombinant proteins tagged with green fluorescent proteins (GFP) in CHO-IR cells and investigated intracellular localizations in the presence and absence of insulin stimulation. Only p85α and p85β redistributed to discrete foci in CHO-IR cells, while other isoforms did not. A recent study also demonstrated that GFP-p85α translocates to similar foci in CHO-K1 cells in response to insulin-like growth factor-1 (IGF-1) stimulation [11]. We have demonstrated these isolated foci to be composed of p85 and IRS-1 by immunohistochemistry and western blotting using an immunoprecipitation method, and found the SH3 domain located in the N-terminal portion of p85 to be responsible for the formation of foci with IRS-1. As monomeric p85 was previously demonstrated to down-regulate insulin signaling by competing with the p85-p110 dimer for IRS-1 binding [12], the formation of p85-IRS-1 foci is likely to be involved in the mechanism of negative regulation of insulin signaling.

Materials and methods

cDNA constructs of each PI 3-kinase regulatory subunit isoform. Rat cDNAs encoding the full-length amino acid sequences of p85α, p85β, p55α, p55γ, and p50α [13], as well as the GFP cDNA (CLONTECH, Laboratories, Inc.) at each N-terminus, were ligated into the EcoRI sites of pSRα vectors. cDNA of the SH3 domain deletion mutant (SH3D) of p85α was prepared as previously described by PCR methods [14] and similarly inserted into pSRα vectors. Fragments prepared by PCR were fully sequenced and observed to have no unexpected mutations.

Cell culture and transfections. CHO-IR cells were maintained in DMEM with 4500 mg/L glucose, containing 10% fetal calf serum (Life Technologies, Inc.) at 37 °C in 5% CO_2. Lipofectamine reagent, Opti-MEM I, was purchased from Gibco-BRL Life Technologies (Eggenstein, Germany). One day before transfection, CHO-IR cells were trypsinized and seeded onto a 60-mm plastic culture dish at 6×10^5 cells/dish. The following day, the transfection procedures were performed using 30 μl of lipofectamine diluted in 300 μl of Opti-MEM I and 6 μg of plasmid DNA diluted in 300 μl of supplemental Opti-MEM-I per 60-mm dish. Cells were incubated in the presence of the lipofectamine-DNA mix for 5 h at 37 °C, in 5% CO_2, and then incubated overnight in DMEM-10% FCS. Forty-eight hours after transfection, each transfected 60-mm dish was used for experiments.

Antibodies and Western blotting. Western blotting was performed as previously described [15]. Commercial antibodies against murine GFP (Chemicon International, CA), phospho-Akt (Ser 473) (Cell Signaling Technology, CA), phophotyrosine, 4G10 (Upstate Biotechnology, NY), and IRS-1 (Cell Signaling Technology, CA) were purchased. After blotting with the indicated secondary antibody, detection was performed using an ECL chemiluminescent kit (Amersham Pharmacia Biotech, UK). Quantitations were performed using a Molecular Imager (Bio-Rad Lab, CA). Immunoprecipitation was performed as previously described [16], using anti-IRS-1 and GFP antibodies. Immunoprecipitates were then boiled in Laemmli sample buffer, subjected to SDS–PAGE, and finally to Western blotting using the anti-phosphotyrosine (4G10) or GFP antibodies.

Immunofluorescence analysis. Immunofluorescence studies were performed as previously described [15]. Cells were plated at near-confluent density on glass coverslips and fixed in 4% paraformaldehyde–PBS for 20 min at room temperature. Coverslips were washed three times in PBS,

then quenched for 15 min in 0.2% Triton X-100. After a further three washes in PBS, coverslips were blocked for 30 min in 2% horse serum-PBS and then washed twice in PBS. Commercial primary antibodies against IRS-1 (Cell Signaling Technology, CA), insulin receptor (Santa Cruz Biotechnology, Germany), Caveolin (BD Biosciences, CA), and p110α [17] were used. These antibodies were diluted in 0.1% horse serum-PBS, and incubations were carried out at 4 °C overnight. Tetramethyl rhodamine isothiocyanate (TRITC)-conjugated anti-mouse immunoglobulin secondary antibody (Zymed Lab., CA) diluted in 0.1% horse serum–PBS was applied after three 5 min washes in PBS. After 1 h of incubation, at RT, coverslips were washed three times in PBS for 5 min each and then mounted in 1% propyl gallate–50% glycerol–PBS and finally observed under a microscope.

Method of deliverying peptides into CHO-IR cells. We delivered peptides into CHO cells using Chariot Transfection Reagent (Active Motif, CA). Briefly, 6 μl of Chariot were diluted in 60% DMSO up to 100 and 100 μl of PBS were added to 50 μg of synthesized proline-rich peptides (PRM1, PPTPKPRPPRPLPVAP). The 100 μl proline dilution was added to the 100 μl Chariot dilution, followed by incubation at RT for 60 min to allow the Chariot-proline complex to form. The cells to be transfected in a six-well tissue culture plate were overlaid with the 200 μl Chariot-proline complex, followed by addition of 400 μl of serum-free medium and incubation for 1hr. Then, we added 1 ml of complete growth medium to the cells and continued the incubation for 1 h. Next, we aspirated the complete growth medium, washed twice with 2 ml of PBS, added serum free medium containing 0.2% BSA and incubated the cells at 37 °C in 5% CO2 for 5 h. After incubation with or without 100 nM insulin for 10 min and washing once with PBS, the cells were fixed with 4% paraformaldehyde for 10 min. After washing with PBS, the cells were observed by fluorescence microscopy. Positive control peptides, 2 μg of β-galactosidase, were transfected into the cells using the same techniques, except for β-galactosidase staining, achieved using a β-galactosidase staining kit (Active Motif, CA).

Results

The schematic structures of five wild-type and one SH3 deletion mutant regulatory subunit isoform of PI 3-kinase are shown in Supplementary Fig. 1. First, we overexpressed wild-type recombinant proteins tagged with GFP in CHO-IR cells and investigated intracellular localizations in both the presence and the absence of insulin stimulation (Fig. 1). Control GFP were found to exhibit intracellular localizations with a greater preference for the nucleus. Interestingly, in contrast to control GFP, p85α, and p85β redistributed to discrete foci in the cells in response to insulin, while they were seen throughout the cytoplasm in quiescent cells. Other isoforms showed no changes in localization with insulin stimulation. The p55α and p55γ exhibited concentrated accumulations around the perinuclear region. In particular, p55γ was restricted to the perinuclear region, while p55α was also distributed throughout the cytoplasm. On the other hand, the distribution of p50α was very similar to that of control GFP.

To investigate the properties of these isolated foci, we searched for proteins co-localized with overexpressed p85-GFP proteins. First, we performed immunofluorescence analyses using antibodies against the insulin receptor, caveolin and the catalytic subunit of PI 3-kinase, p110α, as primary antibodies. However, the signals obtained from these studies were not associated with the foci observed in the cytoplasm when p85α-GFP proteins were overex-